Applied Geochemistry 101 (2019) 1–18

Contents lists available at ScienceDirect

Applied Geochemistry

journal homepage: www.elsevier.com/locate/apgeochem

A strontium ($^{87}Sr/^{86}Sr$) isotopic study on the chemical evolution and migration of groundwaters in a low-rank coal seam gas reservoir (Surat Basin, Australia)

Kim A. Baublys*, Stephanie K. Hamilton, Harald Hofmann, Suzanne D. Golding

School of Earth and Environmental Sciences, The University of Queensland, QLD, 4072, Australia

ARTICLE INFO

Editorial handling by Dr. I. Cartwright

Keywords:
Strontium
Isotopes
Groundwater
Great Artesian Basin (GAB)
Coal bed methane (CBM)
Coal seam gas (CSG)
Methanogenesis
Surat Basin

ABSTRACT

Strontium isotopes, water chemistry and whole rock chemistry have been used to investigate the evolution of water from its surface meteoric composition into methane-rich groundwater. Previous studies established that co-produced Surat Basin coal seam gas waters from the Walloon Subgroup (Queensland, Australia) are meteoric in origin and are distinct across the main production regions but the dominant hydrochemical processes have yet to be determined. In this study, strontium isotope ratios ($^{87}Sr/^{86}Sr$) were measured on production waters from 36 coal seam gas wells, 14 sequentially leached host rock samples and 6 whole rock samples to improve understanding of the water-rock reactions that control spatial variability in solute and isotope chemistry.

Strontium isotope ratios of Walloon Subgroup production waters across all production areas are uniformly low in value, ranging from 0.70338 to 0.70456. The majority of values are significantly lower than shallow Walloon formation waters in the recharge zone and extend the lower range of $^{87}Sr/^{86}Sr$ ratios recorded for Surat Basin groundwaters. These very low $^{87}Sr/^{86}Sr$ ratios (0.70338) are reached early along the flow paths, within 10 km of the shallow recharge area waters, before then undergoing a gradual increase with flow distance. Mineralogical and geochemical analyses of whole rock samples representing each of the main lithologies across the Walloon Subgroup has identified that the low $^{87}Sr/^{86}Sr$ ratios are not derived from any one interval but rather the combination of the same few minerals that are present in every unit.

The rapid accumulation of relatively non-radiogenic strontium early in the flow path across all three gas producing regions has been attributed to a combination of fluid-rock interactions occurring within the Walloon Subgroup itself. Initial surface $^{87}Sr/^{86}Sr$ ratio values are quickly dominated through a combination of processes whereby recharge waters with low Sr concentrations are absorbed onto montmorillonite clays via cation exchange and this combined with weathering of plagioclase causes a re-equilibration of the groundwater to lower $^{87}Sr/^{86}Sr$ ratios. Strontium ratios then start to slowly increase again with flow distance through silicate weathering of K-feldspars and muscovites, which are present at low levels across the basin. Local geological features such as the Hutton-Wallumbilla fault and the Kogan and Undulla anticlines appear to influence flow paths and consequently water and gas composition.

1. Introduction

Prior to the discovery of significant coal seam gas (CSG) resources in the Surat Basin in the 1990s, geochemical research largely concentrated on the potable water aquifers above and below the more saline, coal bed methane bearing Walloon Subgroup (WSG) (Habermehl, 1980, 1986; Radke et al., 2000). Early research on WSG groundwaters and gases by Draper and Boreham (2006) and Hamilton et al. (2012, 2014a, 2015) explored hydro-geological controls on the sources and distribution patterns of the methane. However, questions remain on the flow paths and geochemical evolution of WSG formation waters. Particularly, the extent and relative importance of fluid-rock interactions versus microbial processes, controls on salinity and the pathways and timing of fluid migration are still not fully understood. Interest in the possibility of in-situ regeneration of microbial methane in Walloon coals and geo-sequestration of CO_2 in sandstone formations below the WSG, coupled with a heavy dependence on potable groundwater from surrounding aquifers make a thorough understanding of the evolution of Walloon formation water paramount.

Co-produced waters from the three main CSG production regions of

* Corresponding author.
E-mail address: k.baublys@uq.edu.au (Kim A.Baublys).

https://doi.org/10.1016/j.apgeochem.2018.12.020
Received 4 June 2018; Received in revised form 7 December 2018; Accepted 14 December 2018
Available online 16 December 2018

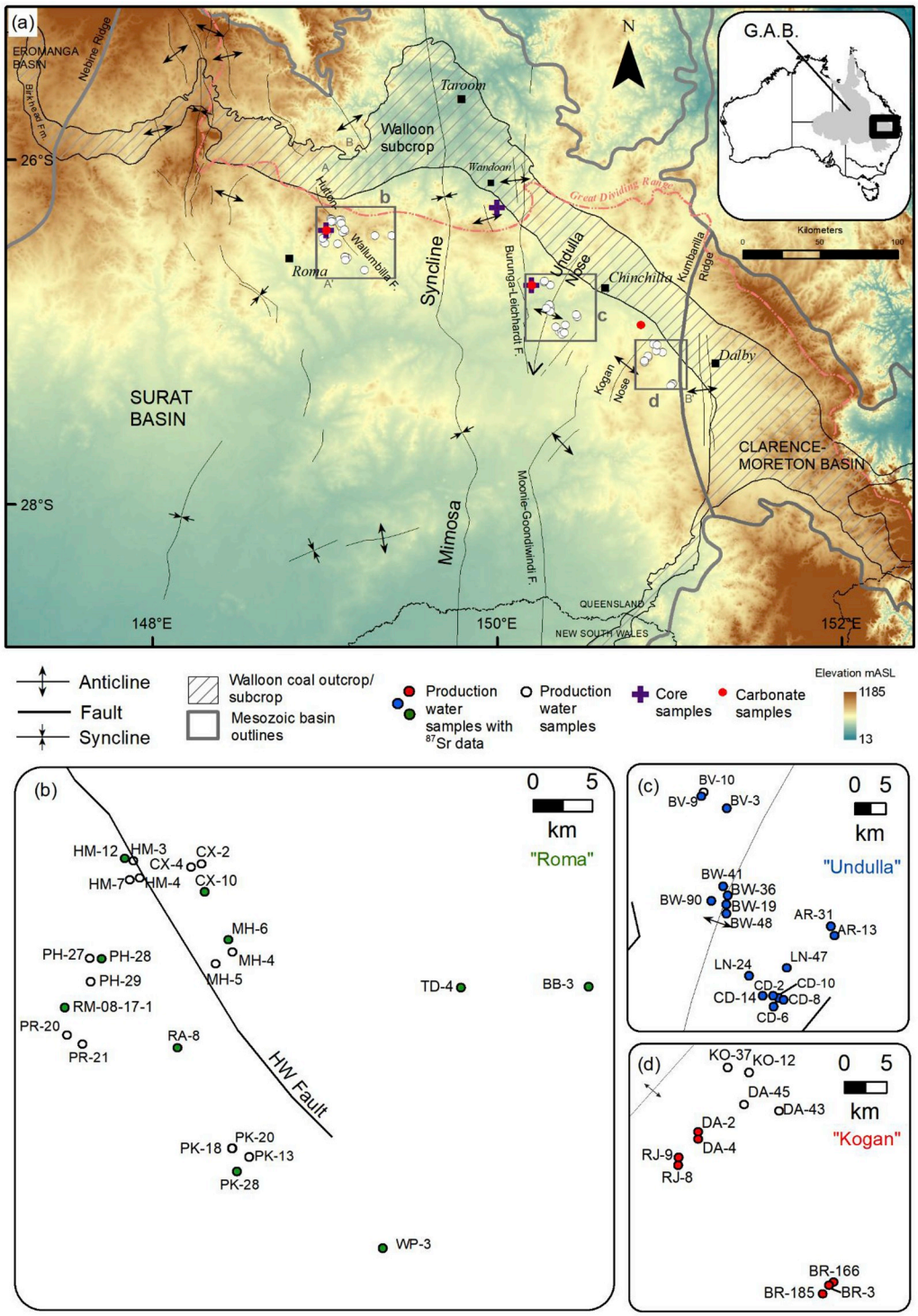

Fig. 1. (a) Structural elements map of the study area, showing the locations of Walloon CSG production water, core and carbonate samples analysed in this study (Baublys et al., 2015; this paper). Inset: Location of the study area within Australia and the Great Artesian Basin (GAB). Lower panels show the names of CSG production water sample locations in the (b) Roma/west, (c) Undulla Nose and (d) Kogan Nose regions. Wells with production water $^{87}Sr/^{86}Sr$ data are represented by filled circles; the fill colours for individual sites are grouped by region and are used throughout the paper to differentiate between groundwater samples from each of these 3 regions.

the WSG are meteoric in origin and have distinct geochemical characters that reflect the initial recharge geology and the coupling of water chemistry and microbial reactions down flow paths (Baublys et al., 2015; Golding et al., 2013; Hamilton et al., 2014a, 2015). Broadly, the groundwater has high Na-Cl-HCO_3 with low SO_4, Mg and Ca as per typical CSG water (Van Voast, 2003). Accessory elements such as F decline in concentration with salinity while Sr and N concentrations increase. The groundwaters display chemical trends with depth, with Cl, alkalinity, δ^2H-H_2O and $\delta^{18}O$-H_2O each behaving differently across the three production areas (Baublys et al., 2015). On the Undulla Nose production fairway in the east, Cl concentrations decrease rather than increase with depth as they do in the western Roma and southeast Kogan Nose areas. Additionally, stable isotope ratios of groundwater on the Undulla Nose are not in line with the rest of the WSG and tend towards more enriched (less negative) $\delta^{18}O$ and δ^2H values with depth versus a depletion in the rest of the basin. On the other hand, alkalinity increases with depth on the Kogan and Undulla Noses while no correlation exists for waters in the Roma area.

In addition to the possibility of subsurface mixing across leaky aquitards or along faults, potential chemical processes influencing WSG water chemistry are evapotranspiration, silicate weathering, carbonate dissolution and/or precipitation and ion exchange with clays and coals.

Alongside the inorganic chemical processes in the WSG are ongoing microbial processes that include CO_2-reducing and acetoclastic methanogenesis along with SO_4 reduction (Evans et al., 2015, Evans, pers. comm., 2017). To explain the changes in WSG water chemistry, inorganic processes need to be decoupled from microbial activity for a better understanding of the controls on water and gas chemistry and therefore gas origins.

Strontium (Sr) can be used as a reactive tracer as it readily substitutes for Ca in carbonates, feldspars and other rock-forming minerals. While Sr concentrations in the water change during mineral formation or mineral dissolution, the $^{87}Sr/^{86}Sr$ isotopic ratio does not undergo fractionation and can be representative of the mineralogy of the host aquifer, allochthonous sediments, or a mix. Hence, Sr isotopes in conjunction with major ion water chemistry can inform on the origin of the solutes and possible flow paths (Frost et al., 2002; Johannesson et al., 1999; McIntosh et al., 2004; Stueber and Walter, 1991). Strontium isotopes have been successfully used to study the regional hydrochemistry of several unconventional gas-bearing basins such as the Illinois (Stueber et al., 1987, 1993), Powder River (Frost et al., 2002; Lemarchand et al., 2015), Michigan (McIntosh et al., 2004) and Appalachian (Capo et al., 2014) basins in the USA. In the Surat Basin, few Sr isotope data exist exclusively for the WSG and most are from groundwater bores where the sampled interval spans two or more Jurassic units. (Collerson et al., 1988; Feitz et al., 2014).

The objective of this study is to identify the major geochemical controls on WSG groundwater chemistry across the three main production areas of the Surat Basin (Undulla Nose, Kogan Nose and Roma). Strontium ion concentration and $^{87}Sr/^{86}Sr$ isotope ratio data for CSG production waters, host rock and host rock leachates are analysed against catchment and basin geology and mineralogical data, combined with pre-existing (Baublys et al., 2015; Feitz et al., 2014; Ransley et al., 2015) and newly collected major ion chemistry and water stable isotope data to identify the water-rock reactions that are responsible for spatial variability in solute and isotope chemistry across the basin. Once the chemical evolution of the waters is better constrained, the microbial influence on the production water can be investigated.

2. Geological and hydrogeological setting

The Late Triassic to Early Cretaceous Surat Basin forms the south-eastern part of the Great Artesian Basin (GAB) and covers approximately 270,000 km^2 of southern Queensland and northern New South Wales. The eastern and northern margins of the Surat Basin form part of the main recharge zone for the GAB (Habermehl, 2002). The Surat Basin evolved in a continental sag setting in the Late Triassic-Early Jurassic (Cook and Draper, 2013). Fluvio-lacustrine strata dominate the lower part of the sequence while the upper part records a marine transgression followed by shallow marine and coastal plain deposition (Exon, 1976).

In our study area in the north-eastern Surat Basin, Walloon Subgroup strata dip gently (< 5°) toward the Mimosa Syncline and range in thickness from < 300 m near Roma to > 500 m east of the Mimosa Syncline (Fig. 1) (Hamilton et al., 2015). The subgroup is relatively undeformed with only minor brittle faults and low-amplitude folds including two anticlines, the Undulla Nose and Kogan Nose, which formed in response to reactivation of the Permian-Triassic Hutton-Wallumbilla, Burunga-Leichhardt and Moonie-Goondiwindi fault systems during and after the Late Cretaceous (Cook and Draper, 2013; Exon, 1976; Hodgkinson and Grigorescu, 2013; Korsch et al., 2009; Scott et al., 2004; Sliwa and Esterle, 2008) (Figs. 1 and 2).

2.1. Lithology and mineralogy

The fluvio-lacustrine Walloon Subgroup is highly heterogeneous, comprising interbedded sandstones (litharenites, commonly with a smectite matrix and carbonate cement), shales, siltstones, mudstones, minor limestones, siderites, silicic ash-fall tuff horizons and coal seams. The coal seams comprise approximately 10% of the whole sequence. The sedimentary beds are laterally discontinuous and difficult to correlate across the basin (Hamilton et al., 2014b; Jell et al., 2013; Martin et al., 2013; Ryan et al., 2012; Scott et al., 2004). The subgroup is commonly divided into six sub-units: a relatively coal-free basal transition unit that is thought to form a laterally extensive aquitard (Durabilla Formation; Hamilton et al., 2014b; Ryan et al., 2012); the Taroom Coal Measures, the Tangalooma Sandstone; and the Juandah Coal Measures, comprising upper and lower informal coal measure members separated by a sandstone interval, informally referred to as the Juandah and/or Wambo Sandstone in the east and the Proud Sandstone in the west (e.g. Hamilton et al., 2014b; OGIA, 2016). It is uncertain whether the sandstone-dominated units act as aquifers or aquitards (cf. Hamilton et al., 2015; Lagendijk and Ryan, 2010; Worley Parsons, 2010), although generally poor sandstone reservoir characteristics and studies of gas distribution and geochemistry tend to support the latter (Hamilton et al., 2014a, 2015). Average coal permeability values range from < 1 to > 500 mD in our eastern study areas, and from ~50 to 200 mD in the Roma/west region, although locally higher values are possible (Ryan et al., 2012; Scott et al., 2007). Walloon Subgroup sandstones generally have poor reservoir characteristics (low porosity, generally < 15%; permeability generally < 2 mD) (Geological Survey of Queensland, 2013; Martin et al., 2013). Overall, there is significant spatial variability across the basin in coal geometry, type and lateral extent (Esterle et al., 2013; Hamilton et al., 2014b; Martin et al., 2013; Ryan et al., 2012), creating the potential for tortuous flow paths.

Walloon Subgroup CSG wells are mainly vertical wells targeting multiple coal seam intervals in both the Juandah and Taroom coal measures. These coal seam intervals are split by very thinly interbedded carbonaceous mudstones and tuff horizons, but more commonly also contain siltstones, claystones and sandstones. As such, CSG water samples tend to be mixtures sourced from several perforated coal seam intervals across at least two Walloon sub-units (Baublys et al., 2015).

2.2. Hydrology and hydrogeology

Spatial variability in recharge to the WSG is not fully understood. Localised recharge (e.g. beneath drainage features), diffuse recharge and flow along preferential pathways (e.g. along faults) are all possibilities (Baublys et al., 2015; OGIA, 2016).

In the study area, streams draining the flanks of the Great Dividing Range traverse the New England Orogen (mafic and felsic intrusives), Surat Basin strata (Triassic-Jurassic siliciclastic sequences), Cenozoic sediments and the Main Range Volcanics (mainly Neogene alkaline olivine basalts). A thick (generally 30–60 m, up to ~130 m; QWC, 2012) Quaternary alluvial aquifer, the upper Condamine River alluvium, obscures most of the Walloon Subgroup recharge zone in the east. Hydraulic heads infer both upward and downward flow between the Walloon Subgroup and the base of the Condamine Alluvium, though interactions are thought to be localised (Dafny and Silburn, 2014; Owen and Cox, 2015). In the Roma/west region, the Walloon outcrop area is largely unobscured by Cenozoic cover allowing direct infiltration into the WSG. The majority of Cenozoic volcanics erupted to the north and east of the Surat Basin and flowed downslope to the study areas; however, it has been suggested that local vents also played a part (Exon, 1976) and geophysical studies suggest that the eastern Surat Basin is an area of high heat flow (Hearn and Webb, 1984; Saygin and Kennett, 2010).

At regional scale, it is generally assumed that groundwater flows toward the central, deeper parts of the Surat Basin; however, local flow conditions may differ and areas of north and east-directed flow have been interpreted in the reservoir and seal units below the Walloon Subgroup (Hodgkinson et al., 2010; KCB, 2017; OGIA, 2016). Groundwater flow is generally to the north on the north side of the Great Dividing Range, i.e. in the Taroom area (OGIA, 2016) (Fig. 1).

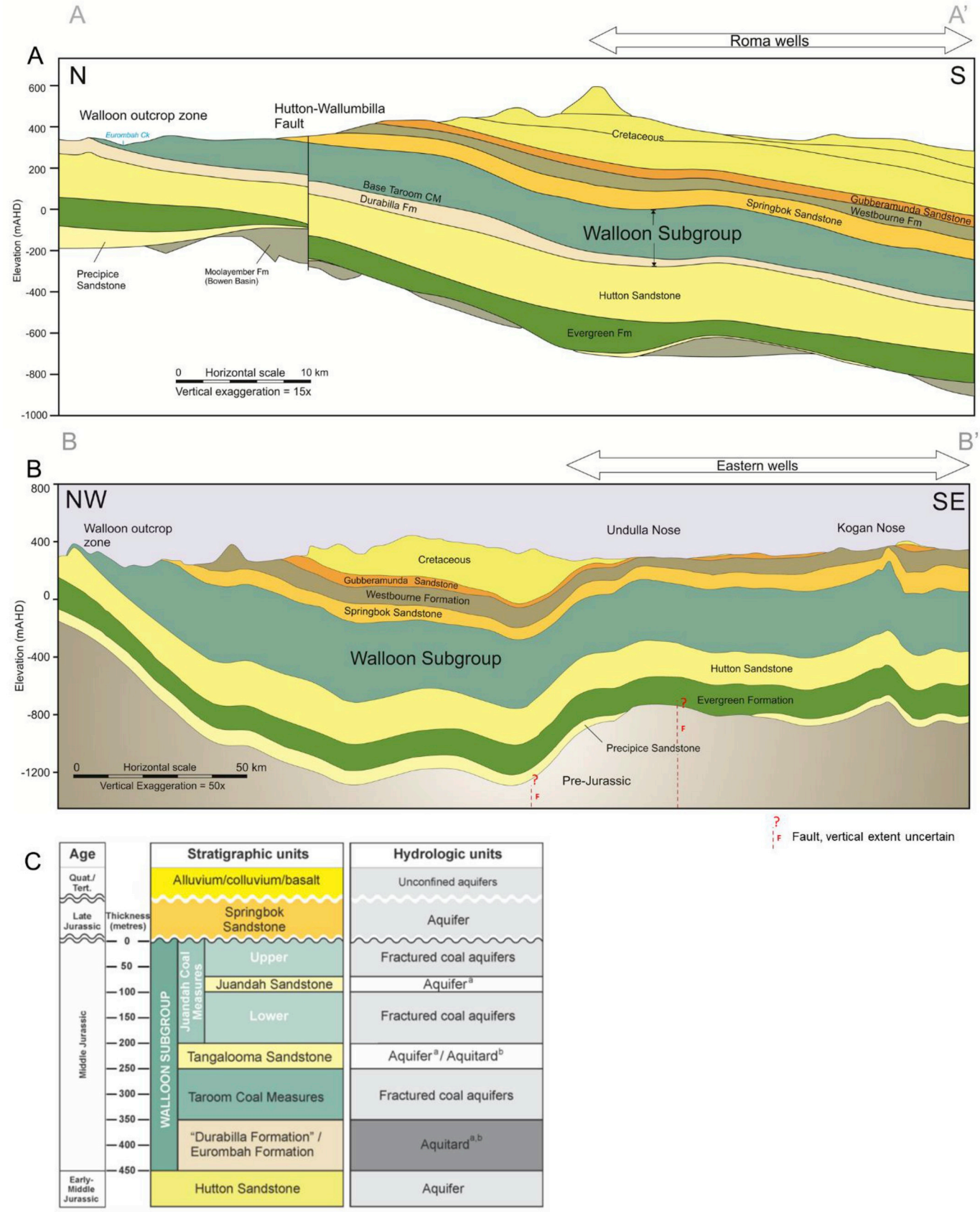

Fig. 2. (a) N-S cross-section through the Roma area (modified from KCB, 2017). (b) NW-SE cross-section along the eastern limb of the Surat Basin (modified from QGC, 2013). See Fig. 1 for section locations. (c) Walloon Subgroup stratigraphic sub-units, hydrologic units and over- and underlying aquifers in the study area. Generalised ages at left from McKellar (1998), [a] Worley Parsons (2010), [b] Lagendijk and Ryan (2010). The sandstone interval separating the Upper and Lower Juandah Coal Measures is informally referred to as the Juandah and/or Wambo Sandstone in the east and the Proud Sandstone in the west.

Table 1
Selected cation and Sr isotope ratios for Walloon Subgroup production waters. (Additional water chemistry available in Appendix Table A.1, A.2).

Well name	Production Interval (m)	Distance (km)	Ca (mg L^{-1})	Mg	Na	K	Sr	$^{87}Sr/^{86}Sr$	Sr/Ca
Undulla Nose									
EAST									
AG-13	261–615	30	3	< 1	1020	4	1.1	0.70384	0.16
AG-31	266–603	29	4	1	1150	5	1.3	0.70449	0.15
BV-3	172–480	14	7	**3**	1670	6	2.4	0.70359	0.16
BV-9	189–527	15	5	**2**	1270	5	1.3	0.70345	0.12
BS-19	362–566	27	2	< 1	825	3	0.5	0.70349	0.12
BS-36	309–617	26	3	< 1	1210	4	1.0	0.70387	0.15
BS-41	307–611	25	2	< 1	740	2	0.4	0.70347	0.10
BS-48	353–668	29	2	< 1	973	3	0.8	0.70368	0.18
BS-90	359–652	28	3	< 1	1020	11	1.0	0.70356	0.15
CD-2	493–782	34	2	< 1	894	4	0.8	0.70369	0.17
CD-14	443–797	44	2	< 1	927	4	0.7	0.70434	0.16
CD-6	468–818	44	3	1	1310	6	1.2	0.70369	0.18
CD-10	465–798	35	2	< 1	1090	4	1.0	0.70356	0.22
CD-8	460–804	42	2	< 1	1000	4	0.8	0.70378	0.19
LN-24	342–649	37	3	< 1	1050	5	1.0	0.70363	0.15
LN-47	403–754	34	3	< 1	935	4	0.9	0.70422	0.14
Kogan Nose									
SOUTH EAST									
RJ-8	316–649	23	10	6	2030	9	4.1	0.70338	0.19
RJ-9	318–663	22	5	4	1960	9	3.1	0.70347	0.28
BW-166	229–528	14	6	2	1440	8	1.6	0.70347	0.12
BW-3	216–546	15	7	3	1540	22	2.0	0.70345	0.13
BW-185	228–573	16	8	4	1740	9	2.4	0.70343	0.14
DV-4	275–623	16	6	3	1600	8	2.1	0.70348	0.16
DV-2	259–601	15	6	3	1780	10	2.3	0.70350	0.18
DAA-43	165–459	10	5	2	1430	5	–	–	–
DAA-45	183–397	13	7	4	1620	9	–	–	–
KO-37	109–298	12	14	5	1950	7	–	–	–
KO-12	34–267	10	28	11	2460	10	–	–	–
Roma									
WEST									
HM-12	393–672	13	6	< 1	1030	15	1.0	0.70344	0.08
HM-3	398–675	13	4	< 1	867	53	0.7	0.70362	0.08
HM-4	388–640	15	4	< 1	797	4	–	–	–
HM-7	395–648	15	3	< 1	780	5	–	–	–
CK-2	175–368	13	4	< 1	691	4	–	–	–
CK-4	196–428	14	3	< 1	747	3	–	–	–
CK-10	200–442	16	3	< 1	782	15	0.4	0.70361	0.07
MH-4	273–509	21	3	< 1	890	6	–	–	–
MH-5	265–515	22	2	< 1	581	4	–	–	–
MH-6	274–489	20	4	< 1	1010	38	0.7	0.70380	0.08
PJ-13	607–843	38	2	< 1	516	22	–	–	–
PJ-18	584–843	38	3	< 1	655	7	–	–	–
PJ-20	675–1048	38	2	< 1	506	7	–	–	–
PJ-28	603–821	40	8	1	1220	5	1.6	0.70409	0.09
PR-20	407–663	29	3	< 1	618	5	–	–	–
PR-21	408–644	29	3	< 1	602	4	–	–	–
PH-27	331–579	22	4	1	665	14	–	–	–
PH-28	356–615	22	4	1	972	125	0.9	0.70372	0.10
PH-29	380–627	24	4	< 1	950	4	–	–	–
RA-8	503–755	29	4	< 1	1080	45	0.9	0.70365	0.10
RM-8	419–662	26	4	< 1	927	24	0.7	0.70383	0.08
BB-3	515–835	32	12	4	1530	86	2.7	0.70351	0.10
WP-3	704–978	48	15	3	1400	31	2.5	0.70353	0.08
TD-4	394–833	29	11	4	1980	31	3.4	0.70361	0.14
Roma surface water			–	–	–	–	–	0.70822	–
Chinchilla surface water (Cobbareena Crk)			–	–	–	–	–	0.70789	–

87Sr uncertainty is ± 0.000010 at 2 σ
Cation ratios are molar
Distance measured from nearest known recharge

Cation concentrations mg L^{-1}
— denotes not measured

3. Sampling and analytical methods

Fifty-one CSG production wells were sampled for water, with 17 news wells being added to the original dataset using the same sampling protocols for collection and storage as the initial study (Baublys et al., 2015). Early field trips did not sample for Sr or ^{87}Sr, as such many of these wells were resampled (sampling dates available in extended table A1 included in the appendix). Additional wells were selected to provide better geographical coverage of the production areas and to fill in sampling gaps such as existed for the Kogan Nose production area of the

Table 2
$^{87}Sr/^{86}Sr$ ratios and selected major element data for Walloon Subgroup whole rock samples: sandstone, siltstone, tuff and clay intervals.

Well site	Depth (m)	Production stratigraphy	K (mg kg^{-1})	Mg	Mn	Na	Ca	Sr	Rb	$^{87/86}Sr$	Sr/Ca (molar)	Rb/Sr (molar)
UNDULLA NOSE												
CH-4	243.68	**Westbourne** (clay)	956	9979	115	24,068	9422	514	12	–	0.02	0.02
CH-4	257.4	**Springbok** (sandstone)	16,580	3700	182	27,377	17,174	397	65	0.704170	0.01	0.17
		Walloon Subgroup										
CH-4	287.3	Juandah (Tuff)	7690	6916	128	25,801	11,857	426	33	0.703814	0.02	0.08
CH-4	363.97	Juandah (clay)	2898	3366	17	7011	1984	272	13	0.703581	0.06	0.05
CH-4	449.2	Juandah (sandstone)	8674	5286	158	5975	1200	224	46	–	0.09	0.21
CH-4	521.38	Tangalooma (sandstone)	13,648	7583	174	18,021	5865	**669**	48	0.704017	0.05	0.07
CH-4	641.44	Taroom(sandstone with siderite)	5756	8724	7601	6342	55,322	167	35	0.705923	0.001	0.22
CH-4	707	Taroom (sandstone)	14,044	3270	457	17,280	14,521	227	63	0.707790	0.01	0.28
ROMA		**Walloon Subgroup**										
PH-25	407.45	Proud (sandstone)	10,955	6304	593	25,134	49,984	**703**	39	–	0.01	0.06
PH-25	582.3	Taroom (siltstone)	17,433	6126	164	7154	2795	**264**	115	–	0.04	0.45
WANDOAN		**Walloon Subgroup**										
GG-2	158	Juandah (clay)	5143	3398	24	4812	2255	**152**	23	–	0.03	0.15
GG-2	158.7	Juandah (siltstone)	16,834	4565	161	10,648	2975	**227**	116	–	0.03	0.52

2σ = ± 0.000009 — denotes not measured.

basin. This paper presents new chemical and tracer data for the additional 17 wells including Sr ($^{87}Sr/^{86}Sr$) isotope analyses. Initial gas isotopic, hydrochemical and groundwater tracer data ($\delta^{13}C$-CH_4, δ^2H-CH_4, $\delta^{13}C$-CO_2, $\delta^{18}O$-H_2O, δ^2H-H_2O, total alkalinity, Na, Ca, Mg, Cl, SO_4, F, N, P, Sr, $\delta^{13}C_{DIC}$, pmC, ^{14}C) for 41 CSG production wells were presented in Baublys et al. (2015). Consistent with the larger dataset, these new production water samples are co-mingled samples sourced from multiple coal seam intervals across two or more Walloon sub-units (Table 1; Fig. 2c).

Whole rock samples from different lithological intervals within the Walloon Subgroup were subjected to whole rock digestion with subsequent analysis of cations (including Rb and Sr) and $^{87}Sr/^{86}Sr$ ratios, and/or a two-stage sequential leach with the leachates analysed for $^{87}Sr/^{86}Sr$ ratios. Samples of Walloon coal and interburden (sandstone, siltstone, tuff, claystone and coal cleat calcite) were collected from 2 cored wells on the eastern (Undulla Nose, CH-4) and western sides of the Mimosa Syncline (Roma, PH-25). Additional coal samples were obtained from a third well in the Wandoan area (GG-2), close to the recharge zone (Fig. 1). Some larger samples could be processed through both experiments; otherwise samples for whole rock digestion and analysis were taken from as close to the leaching experiment sample depths as practical. In addition to the set of WSG samples, additional samples were taken from the overlying Springbok Sandstone and Westbourne Formation in CH-4. Samples were obtained from open-file cores held at the Geological Survey of Queensland Exploration Data Centre, Brisbane. Lithologies sampled were coal (n = 6), sandstone (n = 10), siltstone (n = 3), tuff (n = 3) and cleat carbonate (n = 3), with lithological and stratigraphic information detailed in Tables 2–4.

3.1. Production water sampling

All groundwater samples were collected from actively pumping or free-flowing methane production wells. Roma samples were taken directly from the well-head and the Undulla and Kogan Nose samples were taken either from the separator or from the overflow pipe. Samples were collected from free-flowing water streams after pH, conductivity and temperature measurements had stabilised. All samples for $^{87}Sr/^{86}Sr$ ratio analysis were filtered (0.45 μm) upon collection into acid washed LDPE bottles and acidified with double distilled nitric acid then kept chilled until analysis. In this study, we group the formation

Table 3
XRD mineral compositions of whole rock samples. Sample location details the named WSG interval and brackets denote which drill hole. Interburden ID refers to rock type and depth at which sampled.

Sample Location	Interburden ID	Mineral Composition								
		Qtz	Kaolinite	Montmorillonite	Plag	Calcite	K-feldspar	Chlor	Musc	Siderite
Undulla Nose (CH-4)										
Westbourne	clay @ 243.7 m	–	–	98	–	–	–	–	–	–
Springbok Sandstone	ss @ 257.4 m	24	4	12	57	–	–	2	–	–
WSG - Juandah	tuff @ 287.3 m	22	5	73	–	–	minor	–	–	–
WSG - Juandah	clay @ 364.0 m	11	67	20	–	–	–	–	–	–
WSG - Juandah	ss @ 449.2 m	35	45	8	8	–	–	–	–	–
WSG-Tangalooma SS	ss @ 521.4 m	48	7	21	20	–	–	–	–	–
WSG - Taroom	ss/sid @ 641.44	8	10	–	–	4	–	–	–	75
WSG - Taroom	ss @ 707 m	47	8	9	23	3	–	3	7	–
Roma (PH-25)										
WSG- Proud SS	ss @ 407.5	42	9	13	22	8	–	6	–	–
WSG - Taroom	silst @ 582.3	43	15	14	15	–	–	7	7	–
Wandoan (GG-2)										
WSG - Juandah	clay @ 158.0	23	67	10	–	–	minor	–	–	–
WSG - Juandah	silst @ 158.7	61	8	8	10	–	–	–	13	–

plag = plagioclase sid = siderite — denotes below detection ss = sandstone silt - siltstone chlor = chlorite musc = muscovite

Table 4
Whole rock, sequential leachate $^{87}/^{86}Sr$ ratios.

Well site	Depth	Production stratigraphy (sample mineralogy)	$^{87/86}Sr$ **NH_4OAc**	$^{87/86}Sr$ **Acetic acid**	Total Sr **(ppm)**
UNDULLA NOSE					
CH-4	257.42	Springbok (sandstone) - not in WCM	0.703738		32.0
				0.703735	2.2
CH-4	287.32	Juandah (tuff)	0.703699		21.7
				0.703711	9.5
CH-4	287.66	Juandah (tuff)	0.703711		22.7
				0.703701	8.6
CH-4	363.97	Juandah (coal)	0.703400		4.9
				0.703400	0.9
CH-4	521.38	Tangalooma (sandstone)	0.703370		65.7
				0.703382	3.3
CH-4	637.44	Taroom (coal)	0.703858		4.9
				0.703844	0.5
CH-4	641.44	Taroom (SS with siderite)	0.704296		7.5
				0.704109	6.3
CH-4		Cleat calcites *		**0.7034-0.7040**	
ROMA					
PH-25	366.31	Juandah (coal)	0.703796		6.8
				0.703802	0.5
PH-25	407.45	Proud SS (sandstone)	0.703538		53.6
				0.703553	33.4
PH-25	582.32	Taroom (siltstone)	0.704607		39.8
				0.704609	5.6
PH-25	583.64	Taroom (coal)	0.704419		0.3
				0.704475	0.0
PH-25	583.65	cleat calcite	—	0.704511	
WANDOAN					
GG-2	275.3	Juandah (coal)	0.703304		11.4
				0.703297	2.7
GG-2	486.3	Taroom (coal)	0.703732		9.3
				0.703689	1.5

2σ ± 0.00001, NH_4OAc = ammonium acetate
Sr concentrations were reconstructed from Sr isotope screening data
* Data from Ye 2015

waters by production location (e.g. Undulla Nose) owing to statistically significant differences in their elemental and isotopic water chemistry (see Baublys et al., 2015). Charge balance error (CBE) ranges from 0.1 to 4.8 with an average of 2.4.

In addition to production water sampling, 2 surface water samples were collected from ephemeral creeks after overnight rain.

3.2. Sequential leaching of core samples

To investigate potential sources of the unradiogenic $^{87}Sr/^{86}Sr$ ratios measured in the production waters and to better constrain the 87Sr/86Sr ratio values, coal and interburden samples from three cored wells (CH-4 – Undulla Nose; PH-25 – Roma; GG-2 – Wandoan, Figs. 1, 2 and 6) were subjected to a two-stage sequential leach, with the leachates analysed for $^{87}Sr/^{86}Sr$ ratios. The first leach was ammonium acetate with a neutral pH intended to remove only the adsorbed, easily exchangeable ions (soluble salts, low charge ions), while the acetic acid leach would dissolve any disseminated carbonate material within the coals as well as any carbonate inclusions found in any of the clay minerals.

For coal and interburden samples, all visible carbonate (cleat and vein) was removed and then carbonate free samples were washed with deoxygenated MilliQ water to remove any drill mud before crushing to a coarse powder. Five grams of each sample was then subjected to a two-stage extraction. The first stage was a 24-hr tumble leach with 0.1N ammonium acetate (20 mL) solution, adjusted to a neutral pH. Tubes were then centrifuged, and supernatant removed for $^{87}Sr/^{86}Sr$ ratio analysis. The remaining powders were then rinsed with 40 mL of deoxygenated MilliQ water, centrifuged to remove water then tumble leached for a further 24 h in 20 mL of 0.05M acetic acid to dissolve any disseminated carbonate material. Again, the supernatant was removed after centrifugation and analysed for $^{87}Sr/^{86}Sr$ ratios. A single cleat calcite was also taken from each well and analysed for $^{87}Sr/^{86}Sr$ ratio.

3.3. Strontium isotopic analysis ($^{87}Sr/^{86}Sr$)

Sr isotope analysis was performed on subsets of formation waters from the Undulla Nose (n = 20), Kogan Nose (n = 7) and Roma region (n = 12) (n = 39 data points, N = 35 wells in total), and all leachates and 7 whole rocks, by the University of Queensland (UQ) School of Earth and Environmental Sciences Radiogenic Isotope Facility (RIF).

Approximately 15 mL of each water sample was dried down on a 100 °C hotplate. The resultant residue was dissolved with double distilled 15.8N nitric acid and dried down a further two times with increasingly more dilute nitric acid, then finally taken up with 1.5 mL of 2N nitric acid. Samples were then passed through a cation exchange column filled with Eichrom Sr resin (50–100 μm) to separate the Sr from the matrix. The eluent was then dried down for a final time and taken up with 1.6 μL of 0.05N nitric acid ready for analysis.

Sr isotopic analyses of the waters were performed on a VG Sector 54 thermal ionization mass spectrometer (TIMS), using a three-sequence dynamic protocol. Mass fractionation was corrected assuming $^{86}Sr/^{88}Sr$ ratio = 0.1194 with international standard NBS-987 used as a monitor of instrument status. Precision was calculated from 132 analyses (no data outlier exclusion) of NBS-987 since January 2012 and yielded an average of 0.710222 ± 20 (2σ).

Powdered whole rock samples were first ashed overnight at 550 °C to remove any organics with 100 mg of ashed rock weighed into Teflon beakers for digestion with distilled HF-HNO_3 (4:1). Samples were kept at 110 °C for 7 days before being dried down to a residue. Residues were then taken up with double quartz-distilled, concentrated HNO_3 followed by 1:1 HNO_3 and again dried. Samples were then dissolved in a final 8 ml, 5 percent HNO_3 stock solution and passed through the cation exchange column as per the waters above.

Sr isotopic analyses of the whole rocks were performed on a Nu Instrument; Plasma HR multi-collector inductively coupled plasma-mass spectrometer (MC-ICP-MS). To allow for mass fractionation, SRM-987 was measured after every 5 samples with the value normalized to $^{87}Sr/^{86}Sr$ 0.710249.

3.4. X-ray diffraction (XRD) analysis

Random powder, whole rock XRD analyses were performed on a Bruker D8 by the Centre of Microscopy and Microanalysis within the University of Queensland with mineral identification carried out by EVA software. Clay identification and speciation was determined in conjunction with the Brown and Brindley (1984) and Moore and Reynolds (1997) texts. Air dried, finely ground, samples were scanned from 2 to 70° 2 theta to cover both clay and other mineral ranges.

3.5. Major cation analysis of interburden rock samples

A subset of interburden samples were analysed in the Environmental Geochemistry Laboratory within Earth and Environmental Sciences at the University of Queensland for major element cations plus Sr and Rb. Samples were first ignited at 110 °C to determine water content then at 1000 °C to ash and remove organics. Samples were then fused with LiBO4 and fused glass beads were then taken up in 5% nitric acid before measurement on a Perkin Elmer 8300DV ICP-OES. To compensate for matrix effects, international standards (AGV-2 – andesite; JA-2 –andesite; JB-1b and JB-3 – basalts; JGb-2 – gabbro) were used in conjunction with synthetic standards for calibration.

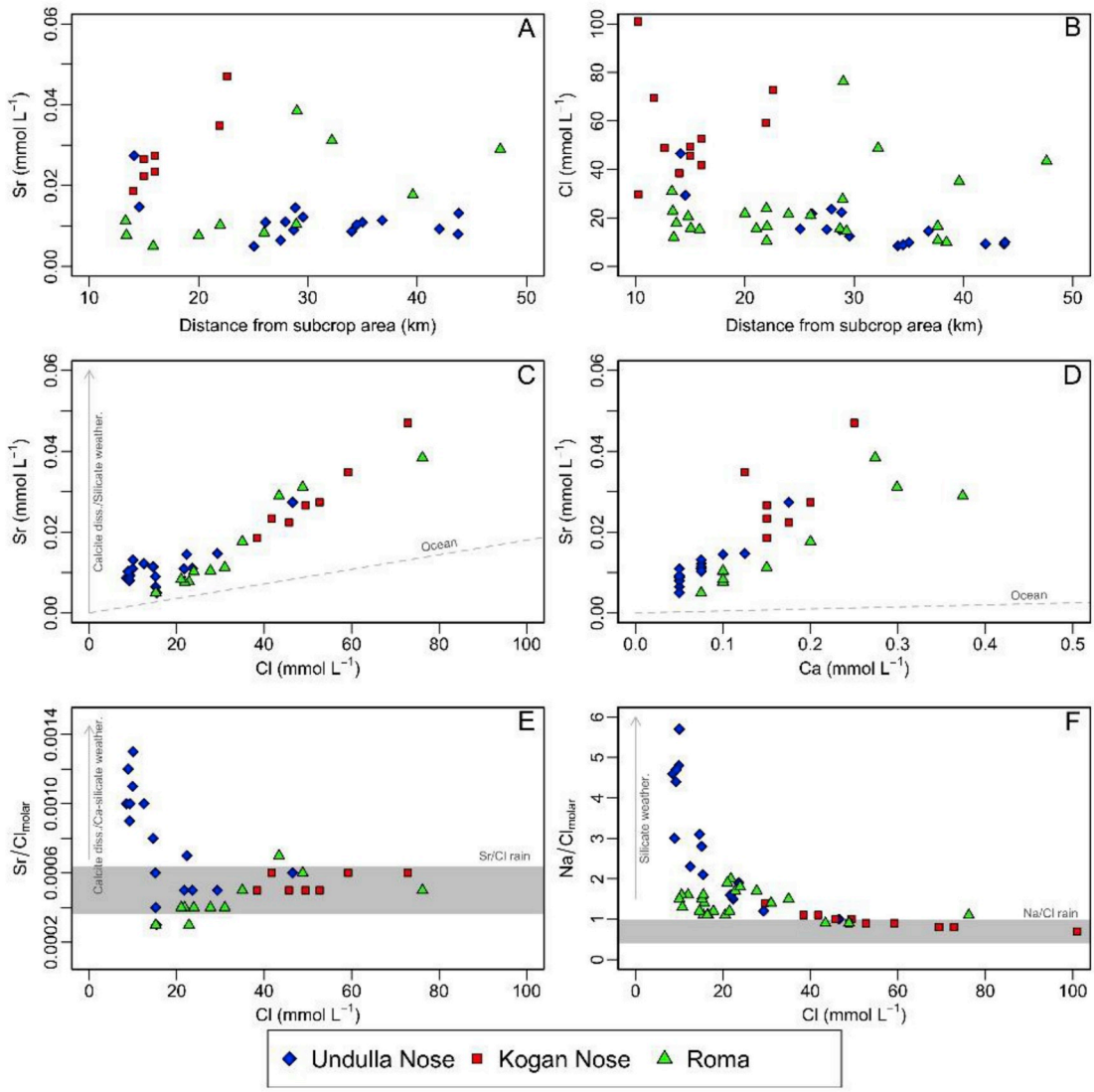

Fig. 3. Molar concentrations and ratios for WSG groundwaters. (a) Sr vs distance. (b) Cl vs distance. (c) Sr vs Cl. (d) Sr vs Ca. (e) Sr/Cl vs Cl. (f) Na/Cl vs Cl. Ocean Sr-Cl and Sr-Ca concentrations (c and d) are adapted from Cartwright et al. (2007). The grey shaded areas in e and f indicate the range of Sr/Cl ratios and Na/Cl ratios in rainfall.

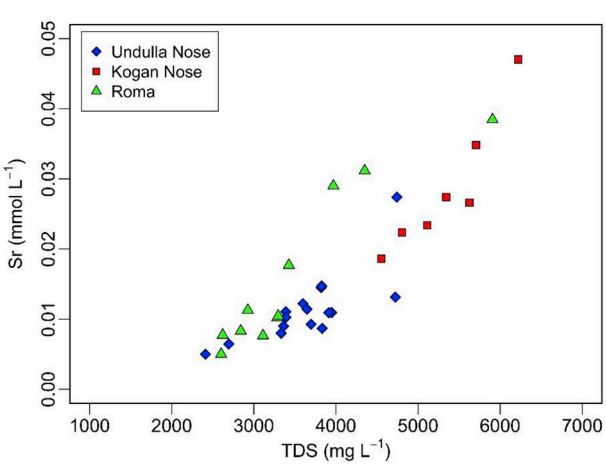

Fig. 4. Strontium molar concentrations versus total dissolved solids (TDS, mg L^{-1}) for the three production areas.

4. Results

All groundwater data in the context of this work refers to methane-bearing, production water sampled directly from a producing CSG well.

4.1. Major ion hydrogeochemistry

All gas wells across each of the three production regions in this study are located between 10 and 50 km from their assumed recharge zones (Fig. 1), with the co-produced water in each region having distinct geochemical characteristics, influenced by differences in the geology of the recharge areas (Baublys et al., 2015, Fig. 2). The western Roma wells have groundwaters that are the freshest with the lowest total dissolved solids (TDS) ranging from 1433 to 5906 mg L^{-1} (average 2738 mg L^{-1}) and low alkalinity ($CaCO_3$), ranging from 372 mg L^{-1} to 1090 mg L^{-1}, average 788 mg L^{-1}. In contrast, the shallower, Undulla Nose groundwaters on the eastern side of the basin have moderate TDS values (average 3645 mg L^{-1}) but double the alkalinity (average 1566 mg L^{-1}) of Roma and a Na excess (defined as additional Na after average rainfall composition). The south-eastern Kogan Nose wells are the shallowest of the three production areas (Table 1) and have the

highest TDS and mid alkalinity values (average TDS: 5286 mg L^{-1}; average alkalinity: 1247 mg L^{-1}). Here, the groundwaters are Na-Cl dominant type, whereas the Roma region and Undulla Nose groundwaters are predominantly of Na-HCO_3 type.

Around the Undulla Nose, Cl concentrations range from 303 to 1650, averaging 603 mg L^{-1} along the assumed flow path and decrease rather than increase with depth and distance ($r^2 = -0.69$) as they do in the Roma and Kogan Nose areas, where concentrations range from 355 to 2700 and 1050–3580 mg L^{-1}, respectively (Fig. 3b). There is a strong positive correlation between Cl and distance along the flow path for most of the Kogan Nose wells (r^2 0.79, Fig. 3b), except for the 2 KO wells that are the shallowest within the Kogan Nose area, and only screened in the Juandah coals (Compare with Fig. 1a, d). There is no correlation between Cl with distance from subcrop for most Roma production waters with only a slight increasing trend, which is mainly caused by the 3 wells located away from the Hutton-Wallumbilla fault. These wells have elevated Cl levels (average of 1990 mg L^{-1}) when compared to the rest from the Roma region (average of 668 mg L^{-1}).

WSG groundwaters also contain lower concentrations of major ions when compared to other sedimentary basins in the world. Ca (median Ca = 5 mg L^{-1}) and Mg levels in particular have been identified as being low (Baublys et al., 2015), compared to other basins (Ca averages, Illinois: 36 mg L^{-1}, McIntosh et al., 2002; Black Warrior: 231 mg L^{-1}, Pashin et al., 2014; Powder River: 30 mg L^{-1}, Rice et al., 2008), while Sr concentrations (avg. 1.3 mg L^{-1}) are comparable with the Powder River Basin (< 1 mg L^{-1}, Frost et al., 2002) and lower than the Black Warrior Basin (13 mg L^{-1}, Pashin et al., 2014).

4.2. Strontium ion geochemistry of production waters

Dissolved Sr concentrations range from 0.437 to 4.12 mg L^{-1} across the three production areas (Table 1). Median Sr concentrations are highest on the Kogan Nose (2.33 mg L^{-1}, n = 7), whereas the Undulla Nose and Roma areas both have less than half with 0.96 mg L^{-1} (n = 16) and 0.92 mg L^{-1} (n = 11), respectively (average values are: 2.5, 1.0, 1.4 mg L^{-1}, respectively). Sr concentration is strongly correlated with distance from subcrop for the Kogan Nose production waters ($r^2 = 0.9$, Fig. 3a, Table 1). In the Kogan Nose recharge area, the Walloon Subgroup is obscured by the Condamine Alluvium. The Condamine Alluvium has a complex hydrogeochemistry but in general is relatively high in TDS with a lack of evaporation trends in $\delta^{18}O$ and δ^2H suggesting mostly transpiration as the process for increasing salinity (Martinez et al., 2015; Owen and Cox, 2015). This likely explains the higher Sr concentrations in the WSG due to concentration through transpiration of meteoric water in the alluvium, which is in line with the generally higher TDS and a lack of evaporation trend in O and H water isotope values (Baublys et al., 2015; this study) (Fig. 4, Appendix Figure A1), given recharge from the alluvium into the WSGs.

Roma waters also show an increase in Sr concentration with distance from subcrop with a strong correlation found for wells along the Hutton Wallumbilla fault ($r^2 = 0.79$) (Figs. 1b and 3a). Roma wells near the Hutton-Wallumbilla fault (labelled in Fig. 1b) have generally low Sr concentrations, ranging from 0.4 to 1.6 mg L^{-1} (CX-10, HM-3, MH-6, RM-08, PH-28, HM-12, PJ-28), while the 3 wells away from the fault have the highest Sr concentrations for the Roma area (TD-4, BB-3, WP-3), which are 3.4 mg L^{-1}, 2.7 mg L^{-1} and 2.5 mg L^{-1}, respectively. Undulla Sr concentrations remain constant with distance from subcrop except for the 2 shallower wells (BV-3, BV-9), which have higher Sr concentrations compared to most of the Undulla Nose waters. Across the production areas, the shallow Roma wells are the freshest (TDS = 2738 mg L^{-1}, cf. Undulla Nose = 3465 mg L^{-1} and Kogan Nose = 5286 mg L^{-1}) and have the lowest initial Sr concentrations of the wells closest to their respective recharge zones (Table 1, Fig. 3a).

Strontium increases with increasing Cl for all wells in the three regions (Fig. 3c), with the Kogan Nose and Roma groundwaters exhibiting slowly increasing Sr/Cl ratios (0.0005–0.0006 and 0.0004 to 0.0007, respectively) while the Undulla groundwaters cover a much greater range (0.0003–0.00130) (Fig. 3c). However, Undulla groundwaters show a reverse trend in Cl concentrations when compared to the other regions as they have declining Cl concentrations with distance from recharge, while the Roma and Kogan Nose groundwaters have increasing Cl concentrations (Fig. 3b). This is also reflected in the Undulla groundwater Sr/Cl ratios that exhibit a strong decline with increasing Cl concentrations (Fig. 3e). In addition to the reverse Cl trend, Undulla waters contain excess Na with Na/Cl molar ratios ranging from 1.6 to 5.7 when compared to wells from Kogan Nose and Roma areas (1.1–2.1 and 1.1–2.5 respectively) (Fig. 3f).

4.3. Strontium isotope ($^{87}Sr/^{86}Sr$) geochemistry of production waters

Across the basin, production water $^{87}Sr/^{86}Sr$ ratios range from 0.703382 to 0.704491, which represents a relatively narrow depleted range (Table 1). These values overlap the $^{87}Sr/^{86}Sr$ ratio range of cleat calcite in Walloon coals of the eastern Surat Basin (0.703363–0.704031; X. Ye, unpubl. data, see acknowledgements) and extend the lower range of Surat Basin $^{87}Sr/^{86}Sr$ groundwater values reported by Feitz et al. (2014), which range from 0.703937 to 0.706789 (average 0.705267).

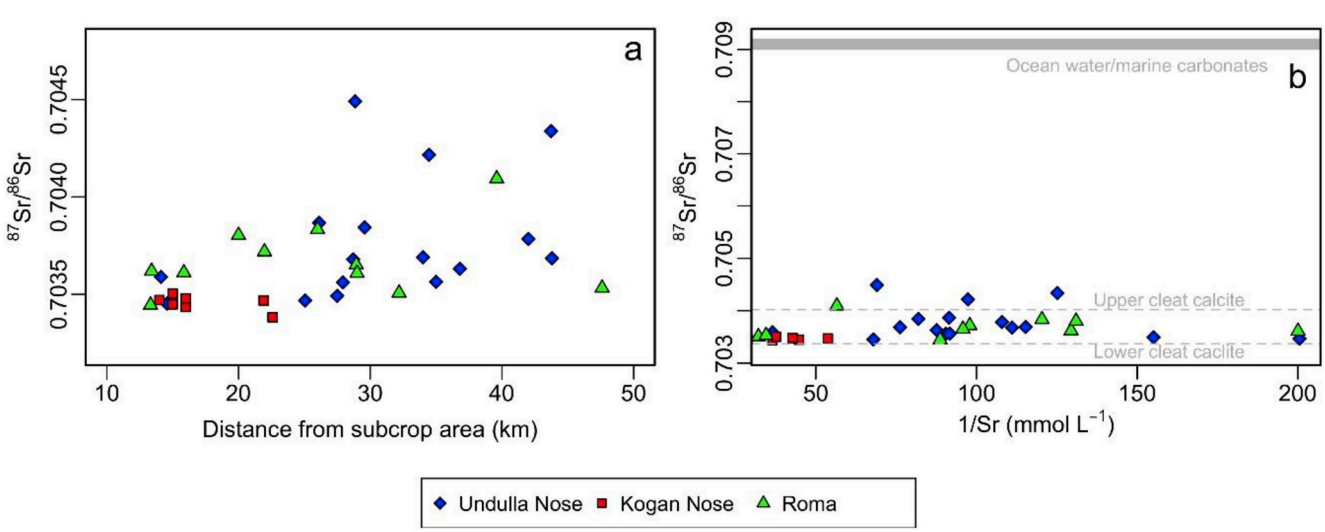

Fig. 5. (a) $^{87}Sr/^{86}Sr$ vs distance to subcrop for WSG production waters. (b) $^{87}Sr/^{86}Sr$ vs 1/Sr (molar).

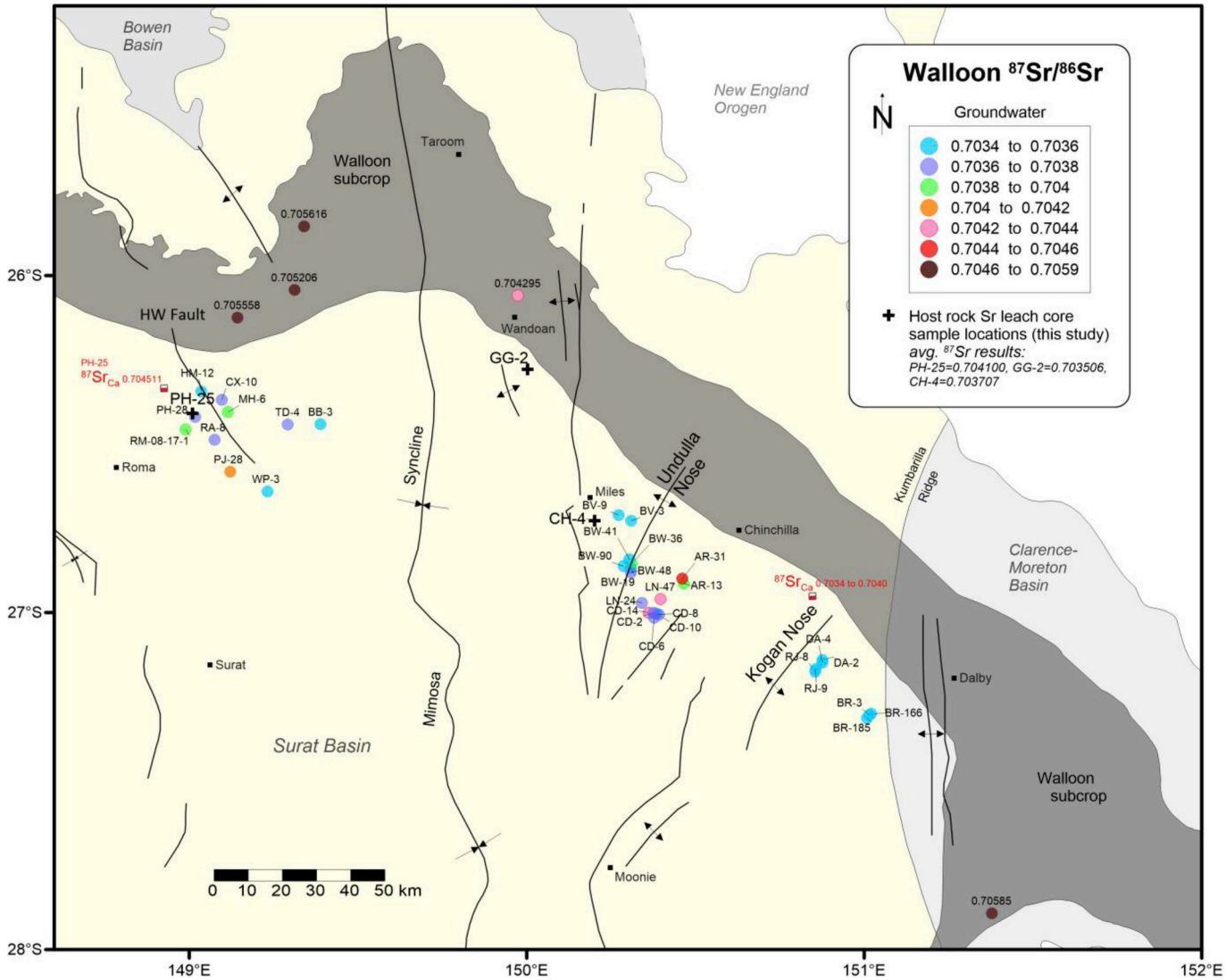

Fig. 6. Map of $^{87}Sr/^{86}Sr$ ratios in groundwater, illustrating spatial variation in relation to CSG production area, the larger sedimentary basins and the subcrop area of the Walloon Subgroup (in dark grey). The abbreviations next to the points (e.g. BB-3) refer to the well names sampled for groundwater in this study. Tectonic structures are presented as major anticlines, synclines and faults. Subcrop area groundwater samples are from Feitz et al. (2014) and were taken from the Walloon Subgroup or Walloon-Hutton interval (range: 0.704295–705616). $^{87}Sr/^{86}Sr_{Ca}$ value range on the Kogan Nose is from X. Ye (unpubl. data, see acknowledgements).

Kogan Nose groundwaters exhibit the narrowest range in $^{87}Sr/^{86}Sr$ ratios, ranging from 0.703382 to 0.703503, have the most depleted median $^{87}Sr/^{86}Sr$ ratio (0.703468) and the highest median total Sr concentrations (2.33 mg L^{-1}) of all three regions, with all wells located close to the recharge zone (Fig. 1a, Table 1). In contrast, Roma and Undulla Nose groundwaters exhibit a greater range in $^{87}Sr/^{86}Sr$ ratios (0.703445–0.704094 and 0.703452 to 0.704491, respectively) and generally lower median Sr concentrations (0.92 mg L^{-1} and 0.96 mg L^{-1} respectively Table 1). In many sedimentary basins, groundwaters become more radiogenic through water-rock interactions the further they move into a basin (Frost et al., 2002), with both the Roma and Undulla Nose waters following this trend (Fig. 5a). The $^{87}Sr/^{86}Sr$ ratios in the Kogan Nose area appear to decrease along the flow path, although the total distance for the transect is only 10 km along the projected recharge path.

All production waters from each region lose their surface or 'initial' $^{87}Sr/^{86}Sr$ ratio signature relatively quickly, generally less than 10 km from the subcrop margin (Fig. 3a). In this context, the majority of Walloon production water $^{87}Sr/^{86}Sr$ ratios are significantly lower than fresh surface waters from Chinchilla ($^{87}Sr/^{86}Sr$ 0.707890), shallower Walloon Subgroup/Walloon-Hutton formation waters in the recharge zone (0.704295–0.705558; Feitz et al., 2014), and rainfall at Chinchilla that is some 400 km inland (0.708224). Overall, $^{87}Sr/^{86}Sr$ ratios are very similar across all three areas, with low $^{87}Sr/^{86}Sr$ ratios for the wells located nearest the recharge areas (Roma 0.70344, Kogan 0.70347, Undulla 0.70353) (Fig. 5a). Kogan Nose $^{87}Sr/^{86}Sr$ ratios remain relatively constant with distance (Fig. 5a), which contrasts with the strong correlation these waters exhibit with increasing Sr concentration with distance from subcrop or recharge area (Figs. 3a and 5a). For the Roma production waters, the $^{87}Sr/^{86}Sr$ ratios increase with distance along the flow path and with Sr concentrations (Figs. 3a and 5a).

Most of the production waters exhibit very little variation in $^{87}Sr/^{86}Sr$ ratios but have a wide range of Sr concentrations (Fig. 5b). The $^{87}Sr/^{86}Sr$ ratios fall within the boundaries of the $^{87}Sr/^{86}Sr$ ratios of cleat calcites in the eastern Surat Basin, which range from 0.7033 to 0.7041 (X. Ye, unpubl. data, see acknowledgements) (Fig. 5b). The few wells with comparatively high $^{87}Sr/^{86}Sr$ ratios are all located in a small area on the eastern flank of the Undulla Nose (Fig. 6).

A recent shallow aquifer interaction study in the Clarence-Moreton Basin to the east also found WSG waters with low $^{87}Sr/^{86}Sr$ ratios (0.70334–0.70431; Duvert et al., 2015). Collerson et al. (1988)

reported similarly low $^{87}Sr/^{86}Sr$ ratios (0.7045–0.7054) for co-mingled groundwater samples from several aquifers including the Birkhead Formation, which is the Walloon equivalent in the recharge area of the GAB in the eastern Eromanga Basin. These waters then become more radiogenic with distance from the recharge area as they flow into the central and discharge regions of the GAB to the southwest (Collerson et al., 1988).

4.4. Whole rock interburden samples: cations, $^{87}Sr/^{86}Sr$ ratios and XRD analysis

Major element cation data from the whole rock cation analysis show that WSG Sr concentrations for the interburden whole rock samples range from 152 to 703 mg kg^{-1}, with the Proud (PH-25) and Tangalooma (CH-4) sandstones containing significantly higher Sr concentrations (703 and 669 mg kg^{-1}, respectively) compared to the other interburden samples (Table 2). The remaining sandstone intervals contained significantly less Sr with concentrations ranging from 167 to 227 mg kg^{-1}. Rubidium concentrations for the whole rocks ranged from 12 to 116 mg kg^{-1}, with the highest levels found in the Taroom (CH-4) and Juandah (GG-2) siltstone samples and the lowest in the two clay samples from the Juandah coal seams (CH-4, GG-2). The Rb/Sr molar ratios for the WSG samples ranged from 0.05 to 0.52, again with the two siltstones having the highest ratio. A pure montmorillonite clay sample from the Westbourne Formation (CH-4) above the WSG had the lowest Rb/Sr molar ratio (0.02) of all samples analysed.

The whole rock Sr/Ca molar ratios for the interburden samples range from 0.001 to 0.09 (Table 2). The siderite-rich sample of Taroom Sandstone from CH-4 had the lowest ratio (0.001), while the sample of Juandah Sandstone also from CH-4 was the highest (0.09). All the Sr/Ca ratios in the rocks are much lower than the Undulla Nose and Kogan Nose production waters (average of 0.16) and have similar values to the Roma production waters (average of 0.09; Table 1).

Whole rock XRD analyses (Table 3) of selected individual samples show that the interburden samples chosen from all three wells contain significant amounts of kaolinite, quartz, plagioclase and montmorillonite. The tuff from CH-4 has the highest Na concentration (Table 2) and appears to be mostly montmorillonite with some minor K-feldspar. The Proud (PH-25) and Tangalooma (CH-4) sandstone samples had minor kaolinite compared to montmorillonite and comprised 20% plagioclase. All the sandstone intervals measured contained plagioclase and montmorillonite, whereas all of the clay-rich samples were dominated by kaolinite and montmorillonite but contained no plagioclase, differing only in the proportions of each. Only the Proud Sandstone contained any detectable calcite although the dominance of clay in the samples made the detection of minor calcite occurrences problematic.

The XRD data agree with previous mineralogical studies of the WSG (Grigorescu, 2011), which have shown that the composition throughout is reasonably homogenous at a high level (with only 4–6 main minerals/lithologies across the whole WSG). Plagioclase (average 17% and up to 47%) is the dominant mineral phase after quartz across all lithologies within the sequence compared to ~5% for the K-feldspars. Kaolinite (~16%) is the dominant clay mineral followed by mixed layer clays (~6%). Minor minerals include calcite and micas. These values represent averages across the whole extent of the WSG and local variations occur. Examination of the wireline logs for all production wells in this study revealed that the ratios of coal, sandstone, mudstone, carbonaceous shale and siltstone are broadly the same across all three sampled areas. The Undulla and Kogan Nose regions are also generally similar in terms of total coal, sandstone, carbonaceous shale and mudstone thicknesses, while the Roma area has half the total thickness of coal and appreciably less of the remaining lithologies. The Westbourne clay (CH-4) sample was found to be composed of almost pure montmorillonite with high Sr (514 mg L^{-1}) and very low Rb (12 mg L^{-1}) and was used as a basis for identification and confirmation of montmorillonite in the remaining samples (Tables 2 and 3).

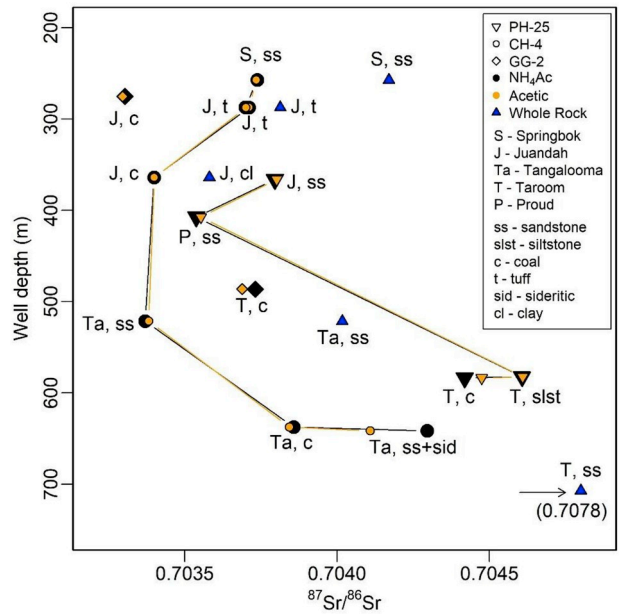

Fig. 7. $^{87}Sr/^{86}Sr$ vs depth for the leachate samples taken from cored wells in the Roma (PH-25), Chinchilla (CH-4) and Wandoan (GG-2) areas. Whole rock samples are from CH-4. Note the Tangalooma (Ta) and Proud sandstone (P) samples have the lowest radiogenic values for their respective wells.

Whole rock $^{87}Sr/^{86}Sr$ ratios were analysed on a small set of samples from the Undulla Nose well (CH-4) and values range from 0.703581 to 0.707790 (Table 2). The tuff and clay interburden samples have $^{87}Sr/^{86}Sr$ ratios like those of the production water ratios with $^{87}Sr/^{86}Sr$ ratios of 0.703814 and 0.703581, respectively. The Taroom sandstone (CH-4) taken from a depth of 707 m has the highest $^{87}Sr/^{86}Sr$ ratio of 0.707790 and consequently had the highest Rb/Sr ratio (0.28, Table 2) of this set. XRD of this sample identified muscovite to be present which is a source of K and thus radiogenic Sr (Table 3). The only other sample to have a relatively high $^{87}Sr/^{86}Sr$ ratio was the siderite-rich Taroom sandstone. The samples which contained the highest proportion of montmorillonite as identified by XRD, also had the highest Sr ion concentrations and the lowest $^{87}Sr/^{86}Sr$ ratios. Additionally, these samples did not contain measurable amounts of plagioclase or calcite, which is another known source of non-radiogenic Sr (Negrel et al., 2001).

In addition to XRD, leaching experiments were conducted on samples from two of the above wells (CH-4, PH-25), with most of the samples selected from the WSG, covering the shallower Juandah and the deeper Taroom coal seams and intervening sandstone intervals (Proud Sandstone in the west and Tangalooma Sandstone in the east), with an additional sandstone selected from the overlying Springbok Sandstone (CH-4). All samples, except for three, had NH_4OAc and acetic acid leach pairs with the same $^{87}Sr/^{86}Sr$ ratios within experimental error (Table 4). The first exception was the Roma Taroom coal where the disseminated carbonate had significantly higher $^{87}Sr/^{86}Sr$ ratios than the associated pore water. Second was the Undulla Nose (CH-4) siderite-rich sandstone sample, where the pore water had a significantly higher $^{87}Sr/^{86}Sr$ ratio than the disseminated carbonate. The third exception was the Wandoan (GG-2) Taroom coal sample where again the pore water leach was more radiogenic than the matching acetic acid leach.

Leachate $^{87}Sr/^{86}Sr$ ratios range from 0.703297 to 0.704609 (Table 4), which cover the full range of the production water $^{87}Sr/^{86}Sr$ ratios (0.70338–0.70456/0.70449, Table 1), although local variations with each of the rock types are evident. The Roma Taroom siltstone leachate (PH-25) had the highest $^{87}Sr/^{86}Sr$ ratio (0.704607) and whole rock XRD revealed this sample contained muscovite in addition to the

ubiquitous kaolinite, plagioclase and montmorillonite found in all samples tested. The Juandah coal leachate from Wandoan (GG-2) contained the lowest $^{87}Sr/^{86}Sr$ ratio (0.703297).

Leachates for the Roma, Proud Sandstone (PH-25) and the Undulla Nose, Tangalooma Sandstone (CH-4) exhibited the lowest $^{87}Sr/^{86}Sr$ ratios for their respective production areas (0.703538 and 0.703370, respectively) and the highest concentration of Sr (703 and 669 mg L^{-1}, respectively; Fig. 7, Table 4). Both wells show a decrease in $^{87}Sr/^{86}Sr$ ratios with depth with the sandstone intervals having the lowest values before increasing again (Fig. 7), which is also reflected in the whole rock data. Coal samples from all three wells showed that the shallower Juandah coal samples had lower $^{87}Sr/^{86}Sr$ ratios than coal samples from the deeper Taroom seams (Table 4, Fig. 7).

5. Discussion

$^{87}Sr/^{86}Sr$ ratios are useful for determining solute sources and likely fluid-rock interactions as ^{87}Sr is only produced by the decay of Rb, which then easily substitutes for K in many minerals, elevating the $^{87}Sr/^{86}Sr$ ratio. ^{86}Sr or non-radiogenic Sr, substitutes for Ca in minerals such as calcite and plagioclase, resulting in a low $^{87}Sr/^{86}Sr$ ratio. Plagioclase and calcite are both Sr-rich and Rb-poor minerals, and waters buffered by these minerals present a source of non-radiogenic Sr (Kendall and McDonnell, 1998) while micas and K-feldspars are a source of higher radiogenic Sr. Once in solution, the $^{87}Sr/^{86}Sr$ ratio is not fractionated and the original host rock isotopic signature is preserved unless more mineral dissolution occurs. This in turns allows $^{87}Sr/^{86}Sr$ ratios to be used to identify likely fluid-rock interactions (Negrel et al., 2017; Petelet-Giraud et al., 2017). In this study, Sr concentrations and isotopes were used to understand the geochemical evolution of water from infiltration along the flow paths into the Surat Basin.

Groundwater flow from the recharge zones to the central parts of a basin induces mineral weathering if the groundwater chemistry is not in chemical equilibrium with the minerals in the aquifer matrix, usually resulting in an increase in major ion content and in many cases, an increase of $^{87}Sr/^{86}Sr$ ratios. Groundwaters from the WSG production sites have unusually low (non-radiogenic) $^{87}Sr/^{86}Sr$ ratios compared to groundwater in similar sedimentary basins. With this study we attempt to answer the following questions: 1) why are the$^{87}Sr/^{86}Sr$ ratios so low; 2) what controls the spatial variation in the $^{87}Sr/^{86}Sr$ ratio geochemistry; and 3) what insights does this provide on basin-scale variability in solute and isotope geochemistry?

While the production waters for each region are chemically distinct from each other, the $^{87}Sr/^{86}Sr$ ratios of all production waters are uniformly low across all three production areas. Moreover, the $^{87}Sr/^{86}Sr$ ratios decrease significantly over a relatively short distance from the recharge zones before slowly increasing along the flow paths as the water moves further into the basin. The mineralogy of the WSG is relatively homogeneous (4–6 minerals dominant) across the basin with only the relative proportions of each mineral (kaolinite, plagioclase, montmorillonite, K-feldspars, quartz) changing within the sandstone, siltstone and mudstone units. It is the differences in the mineral proportions, combined with geochemical weathering processes that are likely responsible for the differences in Sr concentration and $^{87}Sr/^{86}Sr$ ratios across the investigated sites, and the divergence from the recharge values. To explain the distribution of Sr concentrations and $^{87}Sr/^{86}Sr$ ratios, we discuss first the context of the low $^{87}Sr/^{86}Sr$ ratios found in the WSG groundwaters, identify likely Sr sources (whole rock and mineral) and then identify which combination of geochemical processes give the WSG its unique $^{87}Sr/^{86}Sr$ composition.

5.1. $^{87}Sr/^{86}Sr$ ratios and Sr concentrations of Walloon waters in a local and global context

Compared against other studies in the Surat Basin (Feitz et al., 2014), the groundwater $^{87}Sr/^{86}Sr$ isotope ratios from this study span a narrow range (0.70338–0.70449) at the depleted, non-radiogenic end of the scale. Many of these values in the Walloon Subgroup are lower than those of the surrounding aquifers and adjacent recharge zones as well as ratios for Mid-Jurassic seawater (0.707, 175Ma; Clark and Fritz 1997), modern seawater (0.709; Veizer, 1989) and meteoric water (0.708224, 0.70789; this study). Unlike CSG aquifers in USA basins such as the Illinois (marine) (Stueber et al., 1987) and Powder River (non-marine) basins (Frost et al., 2002), which have groundwaters with higher $^{87}Sr/^{86}Sr$ ratios than their corresponding seawater, the WSG groundwaters are less radiogenic than the corresponding seawater values at the time of deposition.

Walloon Subgroup production water $^{87}Sr/^{86}Sr$ ratio values show an initial rapid, strong depletion/decrease from the recharge area to the CSG wells when compared to available rainfall and shallow/surface waters (Fig. 6). This is then followed by a gradual broad increase with depth that is consistent with similar results reported in the literature for the nearby eastern Eromanga Basin section of the GAB (Collerson et al., 1988) and the Powder River Basin CSG play (Frost et al., 2002). $^{87}Sr/^{86}Sr$ ratios are often higher in studies of other basin-scale, silicate-dominated aquifers, such as the Milk River Aquifer, Canada (Armstrong et al., 1998), Riverine Province aquifers of the Murray Basin (Cartwright et al., 2007) and the Algebuckina Sandstone in the SW portion of the GAB in South Australia (Gwynne et al., 2013). In the Algebuckina Sandstone aquifer system, $^{87}Sr/^{86}Sr$ ratios show a uniform decrease with distance from recharge over an approximate 100 km distance from recharge.

5.2. Potential sources of Sr in the WSG

The decrease in $^{87}Sr/^{86}Sr$ ratios from initial recharge values to those found in the production groundwaters occurs over less than 12 km from recharge, suggesting a shallow subsurface source of non-radiogenic Sr in the early stages of flow (Fig. 7). This is reflected in the Sr/Cl molar ratios, which are larger than those expected for seawater/rain water (average Sr/Cl (molar) of seawater ~ 0.0001) (Table 1, Fig. 3c). In sedimentary basins, this can be explained either by a detrital source of non-radiogenic Sr and/or a magmatic source.

Sources of Sr in recharge waters of sedimentary basins include marine aerosols, wind-blown dust from arid central regions, volcanic ash and plant matter through soil uptake (Cartwright et al., 2007). Surface geology, rainfall and evaporation also influence the Sr concentration of surface water. The difference in Sr concentrations across the basin can be attributed to the difference in geology in the recharge areas (Figs. 1, 2 and 6). The area around Roma and the Wandoan, GG-2 well receives recharge directly into the Jurassic basement strata, while the Undulla Nose and Kogan Nose recharge areas comprise Tertiary and Cenozoic sediments, Quaternary alluvium and Tertiary basalts (see Baublys et al., 2015).

Within the WSG, minerals potentially contributing Sr include (in decreasing order of abundance) plagioclase, illite/smectite clays (montmorillonite), alkali feldspars and cleat calcite. Strontium from higher temperature fluids from greater depth also needs to be considered given the Tertiary volcanic history of the basin, and evidence for high heat flow near the Burunga-Leichhardt and Moonie-Goondiwindi fault systems (Hearn and Webb, 1984).

The XRD and geochemical data in this study and the study by Grigorescu (2011) reveal the high amounts of plagioclase and montmorillonite clays in the WSG interburden basin wide to be the most likely mineral contributors of Sr to the groundwater. Plagioclase occurs mostly in the sandstone and siltstone intervals with no evidence of plagioclase in the clay samples. Montmorillonite, however, is contained across all samples. Calcite is also a source of non-radiogenic Sr but the study by Grigorescu (2011) and the results from this study indicate that calcite is only present in minor amounts across the WSG. The mineral source of high radiogenic Sr would be the K-feldspars and micas, as they

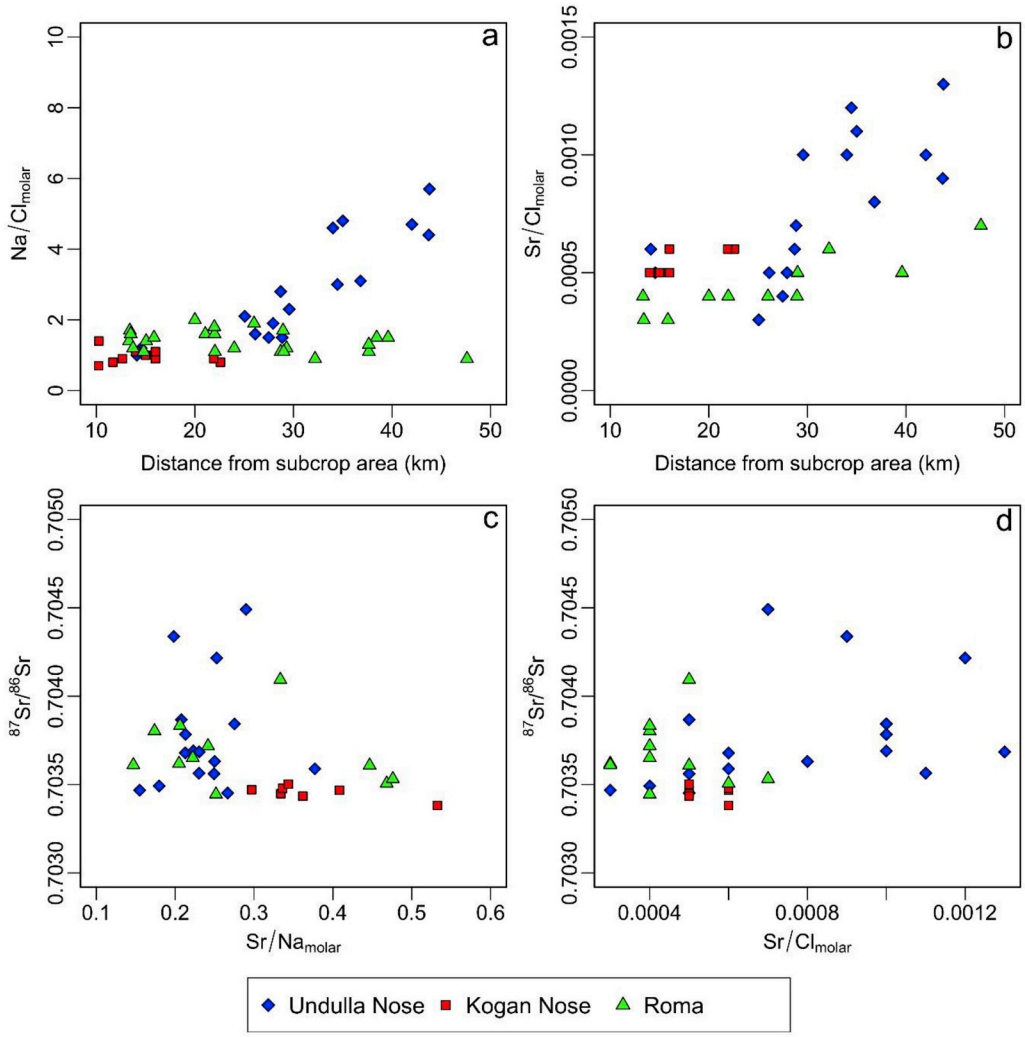

Fig. 8. (a) Na/Cl vs distance. (b) Sr/Cl vs distance. (c and d) $^{87}Sr/^{86}Sr$ vs molar ratios of Sr/Na and Sr/Cl (dissolution of carbonate would show a trend of increasing $^{87}Sr/^{86}Sr$ with decreasing Sr/Na and Sr/Cl ratios).

are a primary source for K and therefore Rb and ^{87}Sr, but both occur only in minor quantities in the basin.

Montmorillonite is most likely the major source of Sr in the WSG as demonstrated by the high Sr (514 mg L^{-1}) and low Rb concentration of the pure montmorillonite sample from the overlying Westbourne Formation, with a Rb/Sr molar ratio of 0.02 (Table 2). Clays such as montmorillonite and coal are exchange phases for cation exchange. Divalent ions are preferably adsorbed over monovalent ions in fresh water. The preference for divalent ions decreases in waters with higher solute content due to complexation of the divalent ions with hydroxyl ion or organic molecules and hence a reduction in the activity of the divalent ions. This can lead to a release of two Na ions for every Sr, Ca or Mg ion that was absorbed.

The siltstones are a source of higher $^{87}Sr/^{86}Sr$ ratios in this case (based on XRD, leaching and whole rock geochemical analysis results), compared to the other rock types (sandstone, tuff, clay), which is supported by the highest Rb/Sr ratio, highest K and significant amounts of muscovite. For example, the Taroom siltstone (PH-25) leachate has the highest $^{87}Sr/^{86}Sr$ ratio (0.704607) of all the rock types analysed (Tables 2 and 4). Consistently, XRD scans indicate that the low $^{87}Sr/^{86}Sr$ ratios for the Proud and Tangalooma sandstone leachates could be due to the high amount of plagioclase and montmorillonite. Given the relative mineral homogeneity across the production areas, and the absence of any other mineral sources, it is likely that the low $^{87}Sr/^{86}Sr$ ratios and small variation within these $^{87}Sr/^{86}Sr$ ratios across the production waters and leachates is heavily influenced by the varying amounts of montmorillonite and plagioclase. In support of this, the Undulla Nose area contains more siltstone, and $^{87}Sr/^{86}Sr$ ratios in the Undulla Nose groundwaters are slightly higher than those for the Roma and Undulla Nose areas.

Although only a minor constituent across the whole WSG, carbonates are still present in some intervals, with whole rock Sr/Ca ratios indicating that the whole rock samples of Roma Proud sandstone (PH-25), Undulla Taroom sandstone and the Undulla Taroom siderite in this study are likely carbonate-dominated. Strontium isotope data from cleat calcites indicates the possibility that the basin on the eastern side of the Mimosa Syncline has been subject to different events or processes compared to the western side of the basin. The sample of cleat calcite from the Roma Taroom (PH-25) coal seam has a higher $^{87}Sr/^{86}Sr$ ratio (0.704544) than all the groundwaters from the Roma region (med. 0.70364), which suggests that the groundwaters and cleat carbonate are not in chemical equilibrium with each other. This is also reflected in the coal leachate from Roma Taroom, whereby the acetic acid leach $^{87}Sr/^{86}Sr$ ratio is significantly higher than the NH_4OAc leach. However, in the east, the cleat calcites from the Undulla and Kogan Nose areas have similar $^{87}Sr/^{86}Sr$ ratios to those of the groundwater (X. Ye, unpubl. data, see acknowledgements), indicating that they are in equilibrium. Equilibrium between the calcite and the groundwater on the east side of the basin could reflect several different events and processes, such as: 1) timing of cleat carbonate formation; or 2) exposure to hotter fluids in

the east, which would speed up equilibration processes.

Collerson et al. (1988) suggested that none of the Jurassic-Lower Cretaceous aquifer sandstones in the eastern Eromanga Basin have an $^{87}Sr/^{86}Sr$ isotope ratio low enough to explain the non-radiogenic $^{87}Sr/^{86}Sr$ values of groundwaters near (< 220 km) the recharge zone, instead highlighting Cenozoic mafic igneous rocks or Paleozoic rocks of the Tasman Fold Belt as possible sources of non-radiogenic ^{87}Sr in hydrologically younger groundwaters. Evidence of the possibility of higher temperatures on the eastern side of the basin has been documented with teleseismic travel-time residuals by Hearn and Webb (1984) indicating the presence of a seismic low-velocity zone at depths of around 150 km beneath the Kogan Nose. These low velocities are interpreted as high temperature anomalies associated with partial melting of the upper mantle. This is also supported by Saygin and Kennett (2010) whose tomographic inversion of ambient seismic noise suggests higher temperatures at depths of ~85 km below both the Kogan Nose and Undulla Nose. The region of elevated temperature under the Kogan and Undulla Noses could have been a source of higher temperature fluids, which is in line with $^{87}Sr/^{86}Sr$ isotope ratios being in equilibrium between the disseminated calcite and the cleat calcite veins. Cleat calcites from the Kogan Nose area have yet to be successfully dated (X. Ye, unpubl. data, see acknowledgements), however Ye (X. Ye, unpubl. data, see acknowledgements) postulated that the cleat calcites in this area formed when hydrothermal fluids mixed with meteoric waters. By contrast, the Roma area lies within a transition zone where the low-velocity zone is less strongly developed (i.e. not as hot). This is consistent with the Roma cleat calcite not being in equilibrium with the disseminated calcite, which is also demonstrated by the higher $^{87}Sr/^{86}Sr$ ratio in the acetic acid leachates than in the NH4OAc leachates from the Roma Proud sandstone and the Roma Taroom coals.

In the east, the small number of production groundwaters with higher $^{87}Sr/^{86}Sr$ ratios (above the range of eastern Surat cleat carbonates) are all located near a fault, on the eastern flank of the Undulla Nose. This may indicate different water-rock interactions at a local scale, or a longer flow path, rather than a direct path from nearest recharge. Hodgkinson et al. (2010) suggested that groundwater in the underlying Hutton aquifer flows northwards rather than west in this area, which may also be the case in the overlying WSG. Other possible explanations are inter-aquifer mixing and direct overhead recharge. There is debate as to whether the major north-eastern fault systems cut the Walloon Subgroup (e.g. Ryan et al., 2012; Willink, 2008 cf. Hodgkinson and Grigorescu, 2013; McKillop et al., 2011). Hodgkinson et al. (2010) interpreted vertical hydraulic communication between the Hutton Sandstone and the Springbok Sandstone through the Walloon Subgroup at one location near the Burunga-Leichhardt fault and suggested that the major Surat Basin faults do not present a barrier to groundwater flow. Conversely, regional groundwater modelling studies have suggested that most of the major Surat Basin faults are likely to restrict flow, especially lateral flow (OGIA, 2016). Given the disagreement, the possibility of upwelling deeper fluids or cross-formational flow should not be discounted. Geochemical and neotectonic data suggest that selected major faults in the GAB act as conduits to deeply-sourced endogenic fluids (Love et al., 2010) and Suckow et al. (2018) suggested that older waters had ascended along the Hutton-Wallumbilla fault into the Hutton Sandstone near our Roma study wells. At local scale, significant small-scale folding and faulting of the WSG is evident from drilling, seismic data and open-cut mine exposures in the eastern Surat Basin (Denis, 2013; Ryan et al., 2012). Together, the latter studies suggest a fault throw range from sub-seismic to 50 m, juxtaposing gas-producing coals against fine-grained baffles, and potentially, over- and underlying aquifer units. Additional geochemical tracer data, such as noble gas components and $^{3}He/^{4}He$ analyses are needed to examine for tectonic sources of solutes and mixing with older basinal waters near fault zones. These data should be collected and coupled with microbiological and tomographic data as part of future research.

5.3. Geochemical fluid-rock processes which influence $^{87}Sr/^{86}Sr$ ratios

Across the WSG, most of the minerals identified above are contained within the sandstone, siltstone and mudstone intervals, which comprise approximately 85% of the subgroup. As such, the geochemical processes likely to be dominant in the WSG are silicate weathering and cation exchange. However, minor occurrences of calcite in some of the sandstone intervals and minor cleat and vein calcite in the coals may have an influence on the $^{87}Sr/^{86}Sr$ ratios and will therefore be discussed as well.

5.3.1. Silicate and carbonate dissolution

Determination of carbonate over silicate weathering uses the same or similar indicators such as Sr/Cl ratios and as such will be considered together. All production water Sr/Cl ratios are higher than ocean water, which suggests that carbonate and/or silicate weathering is occurring (Fig. 3c). However, the absence of an inverse correlation between Sr/Cl and Sr/Na ratios with $^{87}Sr/^{86}Sr$ ratios (Fig. 8c and d) indicates silicate weathering rather than carbonate dissolution. This does not preclude carbonate dissolution occurring at a local level, for example, the similarity between the $^{87}Sr/^{86}Sr$ ratios of the groundwaters and the cleat calcite in the east appears to indicate some carbonate dissolution, as discussed above. Calculated calcite saturation indexes using Phreeqc indicate that calcite is oversaturated in the groundwaters on the eastern side of the basin while the Roma groundwaters on the west are mostly at equilibrium with any calcite present (Table A2) which reinforces that carbonate dissolution is not a dominant process in these groundwaters. The Sr/Ca ratios remain relatively constant with distance from the subcrop area in groundwaters in the Roma area, while Undulla and Kogan groundwater Sr/Ca ratios increase with the largest increase in the Kogan groundwaters. The reason for this is most likely calcite precipitation due to an increase in bicarbonate from methanogenesis processes as the $^{87}Sr/^{86}Sr$ ratios remain constant.

Na/Cl ratios are independent of carbonate dissolution as carbonates contain negligible amounts of Na and Cl but abundant Sr (Dogramaci and Herczeg, 2002). All WSG groundwaters have Na/Cl ratios greater than ocean and meteoric water values indicating silicate weathering, although only the Undulla and Kogan Nose groundwaters show increasing Na/Cl ratios with distance (Fig. 8a). Silicate weathering from sandstones is likely to contribute significant amounts Sr given the mineralogical composition, with high Sr ion concentrations and significant amounts of plagioclase observed in the whole rock samples. Silicate weathering is occurring in the Undulla groundwaters and perhaps to a smaller extent in the Kogan Nose groundwaters but is not evident in the Roma groundwaters (Fig. 8a).

5.3.2. Cation exchange

The variation among $^{87}Sr/^{86}Sr$ ratios in the whole rock sandstone interburden samples within the WSG, wherein some intervals have similar $^{87}Sr/^{86}Sr$ ratios to the groundwaters and some have much higher $^{87}Sr/^{86}Sr$ ratios (e.g. Undulla Nose Taroom sandstone (CH-4)), indicates other geochemical processes such as cation exchange, are occurring in addition to silicate weathering.

All the whole rock interburden samples of the WSG contain significant amounts of the smectite clay montmorillonite (8–21%) in addition to kaolinite (4–69%) (Table 3). Smectitic clays such as montmorillonite and bentonite as well as coals, have large cation exchange capacities, which can influence overall water composition. Armstrong et al. (1998) found that the presence of bentonite levels as low as 10% in aquifer lithologies is enough to cause a significant drop in the $^{87}Sr/^{86}Sr$ ratios of the groundwater. The process of Sr adsorption and exchange with the montmorillonite causes the re-equilibration of the $^{87}Sr/^{86}Sr$ ratios in the groundwater (Armstrong et al., 1998; Cartwright et al., 2007). Overall, all 3 production areas show the influence of progressive cation exchange, which is attributed to the coals and montmorillonite clays present within the WSG.

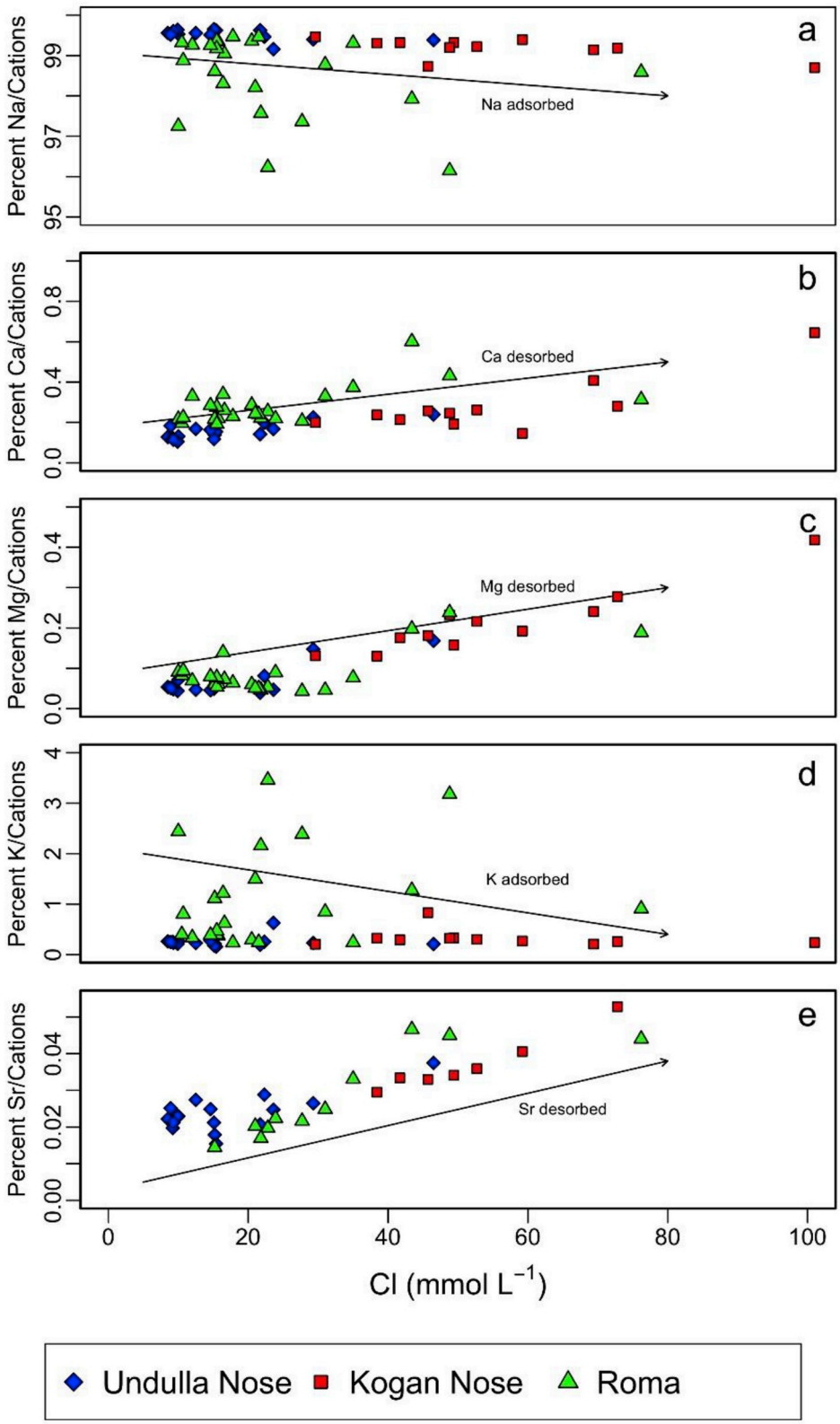

Fig. 9. Relative molar concentrations as a proportion of total cations versus Cl concentrations for WSG groundwater; percent of total cations for a) Na versus Cl, b) Ca versus Cl, c) Mg versus Cl, d) K versus Cl, and e) Sr versus Cl.

Cation exchange experiments on clays by Wahlberg et al. (1965) have shown cation exchange is greatest in waters with a pH 8 and that the best range for exchange is between 8 and 8.5, with a salinity range of 200–400 mg L^{-1}. Most of the groundwaters in the WSG fall within this optimum pH and salinity range, which would allow for maximum cation exchange.

Cation exchange with Na rich montmorillonite releases 2 moles of Na for every mole of Sr/Ca/Mg adsorbed at lower salinities. Almost every groundwater sample in this study has a Na excess, although this is more prevalent in the Undulla Nose waters (Fig. 3f). Changes in the

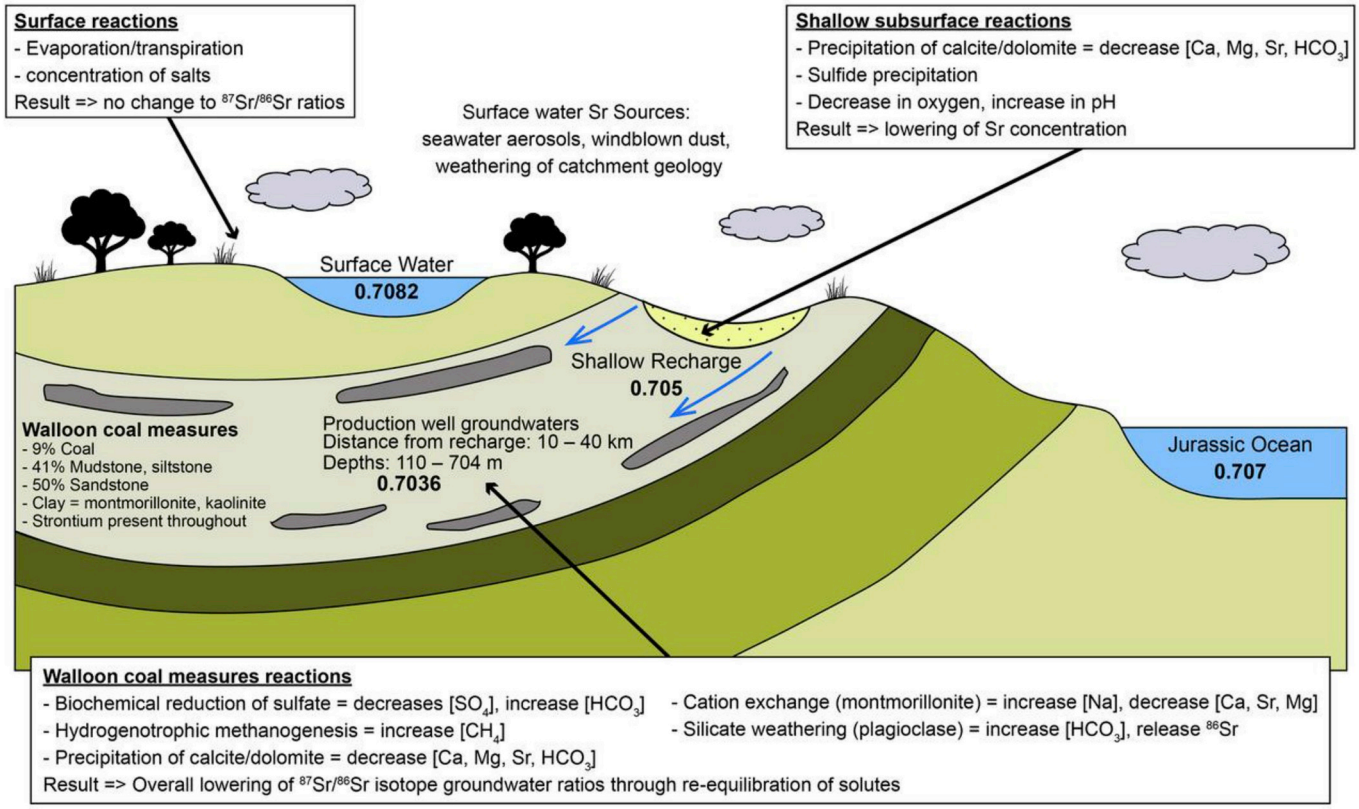

Fig. 10. Summary schematic detailing the geochemical evolution of the strontium isotope ratios of the production well groundwaters of the Walloon coal measures in the Surat Basin.

relative proportion of cations along flow paths can also be used as an indicator of waters undergoing cation exchange processes (Cartwright et al., 2007). Decreasing Na paired with increasing Ca and Mg indicates ion exchange reactions, from mostly divalent ion sorption to a combination of divalent and mono-valent sorption due to the decreasing activity of divalent ions with increasing salinity. Although differences in the relative proportions of cations are small, due to Na representing over 99% of the cations in the WSG, a decrease in Na and an increase in Ca, Mg and Sr with increasing salinity suggests cation ion exchange is occurring across the WSG (Fig. 9).

6. Conclusions

Strontium and Sr isotope chemistry, combined with major ion geochemistry have provided insights into the evolution of the CSG production water chemistry of the Walloon Subgroup (WSG) of the Surat Basin. There are significant regional differences in the basic groundwater chemistry of the three main production areas (Undulla, Kogan, Roma-west), which have been attributed to the different recharge lithologies across the basin. On the other hand, the production water $^{87}Sr/^{86}Sr$ ratios are similar across these three areas, with most ratios being significantly lower than estimated ratios for the recharging meteoric waters. This rapid decrease to non-radiogenic values early in the flow path for all three areas most likely reflects fluid-rock interactions within the WSG itself (Fig. 10).

The gross lithology of the WSG is similar across the basin, with the same minerals present across all lithological intervals and only the proportions of the mineral assembly varying slightly. We conclude that the main mineral source of Sr is plagioclase and montmorillonite, with the highest concentrations of Sr present in the sandstone intervals. Whole rock chemistry and $^{87}Sr/^{86}Sr$ ratios indicated that no single interval could be confidently attributed to influencing the overall low $^{87}Sr/^{86}Sr$ radiogenic values of the production waters.

Of the geochemical processes that influence Sr concentrations and $^{87}Sr/^{86}Sr$ ratios, a combination of silicate weathering and cation exchange are the dominant processes. We further conclude that it is the combination of Sr absorption on coal and cation exchange by clays (montmorillonite) that removes the initial recharge, higher radiogenic Sr from solution, causing a re-equilibration and lowering of the $^{87}Sr/^{86}Sr$ ratios in the groundwater. Faster weathering plagioclase then provides an additional source of non-radiogenic Sr, which results in the rapid decrease of the $^{87}Sr/^{86}Sr$ isotopic ratios with distance from recharge and gives the production waters their uniformly low $^{87}Sr/^{86}Sr$ ratios. Further along the flow paths, the presence of low levels of the slower reacting K-feldspars and micas start to slowly contribute ^{87}Sr to the groundwaters and gradually gain influence over the low $^{87}Sr/^{86}Sr$ ratios.

Local differences in cleat calcite versus disseminated carbonate have been revealed, with a sample of Roma calcite being more radiogenic and not in equilibrium with the production waters, while Undulla Nose groundwaters appear to be in equilibrium with their cleat calcite. This equilibrium in the east has been linked to the presence of a local hotspot which is absent in the west. Local differences are also seen in the Roma area with the Hutton-Wallumbilla fault appearing to influence the water chemistry in that area, with wells away from the fault being more saline.

Traditionally, Sr isotope ratios are often used to indicate recharge and mixing between aquifer units. This study demonstrates the complexity of Sr isotope geochemistry within sedimentary basins and has shown the importance in considering the hydrogeochemical processes occurring along the flow-paths. We have shown that geochemical processes in aquifers can play a significant role in Sr isotope and Sr content distribution. This has implications for the use of Sr (isotopes and content) as a tracer in larger sedimentary basins and while there is still good reason to connect origins of groundwater to Sr isotopes, hydrogeochemical processes along the flow path must be taken in considerations.

Acknowledgements

The authors wish to acknowledge financial and logistical support from QGC – A BG Group Business, Santos Ltd, Total SA and the Australian Research Council (LP100200730). We would like to thank our University of Queensland (UQ) colleagues, particularly A. Hentschel for providing the Wandoan, GG-2 Walloon coal samples and G. Dawson for insightful discussions on Surat carbonates. Thanks to S. Hearn for seismic conversations and J. Pearce for final manuscript review. Thanks to M. Mostert of the UQ Environmental Geochemistry Laboratory for the whole rock elemental analyses and RIF staff and W. Zhou for the Sr isotopic analyses. The UQ Master's thesis by X. Ye assisted the interpretations presented in this paper. We are grateful to the reviewers for their time and insightful comments which improved the manuscript.

Appendix A. Supplementary data

Supplementary data to this article can be found online at https://doi.org/10.1016/j.apgeochem.2018.12.020.

References

Armstrong, S.C., Sturchio, N.C., Hendry, M.J., 1998. Strontium isotopic evidence on the chemical evolution of pore waters in the Milk River Aquifer, Alberta, Canada. Appl. Geochem. 13, 463–475.
Baublys, K., Hamilton, S., Golding, S., Vink, S., Esterle, J., 2015. Microbial controls on the origin and evolution of coal seam gases and production waters of the Walloon Subgroup; Surat Basin, Australia. Int. J. Coal Geol. 147, 85–104.
Brown, G., Brindley, G.W., 1984. Crystal Structures of Clay Minerals and Their X-Ray Identification, second ed. Mineralogical Society, London, pp. 305–360.
Capo, R.C., Stewart, B.W., Rowan, E.L., Kohl, C.A.K., Wall, A.J., Chapman, E.C., 2014. The strontium isotopic evolution of Marcellus Formation produced waters, southwestern Pennsylvania. Int. J. Coal Geol. 126, 57–63.
Cartwright, I., Hannam, K., Weaver, T., 2007. Constraining flow paths of saline groundwater at basin margins using hydrochemistry and environmental isotopes: lake Cooper, Murray Basin, Australia. Aust. J. Earth Sci. 54, 1103–1122.
Clark, I., Fritz, P., 1997. Environmental Isotopes in Hydrogeology. CRC Press, USA.
Collerson, K.D., Ullman, W.J., Torgersen, T., 1988. Ground waters with unradiogenic 87Sr/86Sr ratios in the Great Artesian Basin, Australia. Geology 16, 59–63.
Cook, A.G., Draper, J.J., 2013. Geology of Queensland: 7.5. Surat Basin. Geological Survey of Queensland, Brisbane.
Dafny, E., Silburn, D., 2014. The hydrogeology of the Condamine River alluvial aquifer, Australia: a critical assessment. Hydrogeology 22, 705–727.
Denis, G., 2013. Faulting in the Surat Basin and the Implications for Hydraulic Connectivity. BSc Honours Thesis. Royal Holloway, University of London 67 pp.
Dogramaci, S.S., Herczeg, A.L., 2002. Strontium and carbon isotope constraints on carbonate-solution interactions and inter-aquifer mixing in groundwaters of the semi-arid Murray Basin, Australia. J. Hydrol. 262 (1–4), 50–67.
Draper, J.J., Boreham, C.J., 2006. Geological controls on exploitable coal seam gas distribution in Queensland. APPEA J. 46, 343–366.
Duvert, C., Raiber, M., Owen, D.D., Cendón, D.I., Batiot-Guilhe, C., Cox, M.E., 2015. Hydrochemical processes in a shallow coal seam gas aquifer and its overlying stream–alluvial system: implications for recharge and inter-aquifer connectivity. Appl. Geochem. 61, 146–159.
Esterle, J.S., Hamilton, S.K., Ward, V., Tyson, S., Sliwa, R., 2013. Scales of Geological Heterogeneity within the Walloon Subgroup and its Coal Measures. Technical Report by School of Earth Sciences. University of Queensland for Queensland Department of Natural Resources and Mines, Brisbane Retrieved 11 January 2014. http://www.dnrm.qld.gov.au/_data/assets/pdf_file/0008/106010/act-1-3-final-report-walloons.pdf.
Evans, P., Parks, D., Chadwick, G., Robbins, J., Orphan, V., Golding, S., 2015. Methane metabolism in the archaeal phylum Bathyarchaeota revealed by genome-centric metagenomics. Science 350, 434–438.
Exon, N.F., 1976. Geology of the Surat Basin in Queensland. Bur. Miner. Resour. Geol. Geophys. Bull. 166.
Feitz, A., Ransley, T., Hodgkinson, J., Preda, M., Dunsmore, R., McKillop, J., Spulak, R., Dixon, O., Kuske, T., Draper, J., 2014. GA-GSQ Hydrochemistry Dataset (2009-2011) GEOCAT No. 78549. Geoscience Australia, Canberra.
Frost, C., Pearson, B., Ogle, K., Heffern, E., Lyman, R., 2002. Sr isotope tracing of aquifer interactions in an area of accelerating coal-bed methane production, Powder River Basin, Wyoming. Geology 30, 923–926.
Geological Survey of Queensland, 2013. Queensland Digital Exploration Reports (QDEX) System (Online). Geological Survey of Queensland, Brisbane. https://www.business.qld.gov.au/industries/mining-energy-water/resources/minerals-coal/online-services/qdex-data.
Golding, S.D., Boreham, C.J., Esterle, J.S., 2013. Stable isotope geochemistry of coal bed and shale gas and related production waters: a review. Int. J. Coal Geol. 120, 24–40.
Grigorescu, M., 2011. Jurassic groundwater hydrochemical types, Surat Basin, Queensland - a carbon geostorage perspective. Geological Survey of Queensland Record 2011/05, Report 90013. https://www.business.qld.gov.au/industries/mining-energy-water/resources/minerals-coal/online-services/qdex-reports.
Gwynne, R., Frape, S., Shouakar-Stash, O., Love, A., 2013. 81Br, 37Cl, and 87Sr studies to assess groundwater flow and solute sources in the southwestern Great Artesian Basin, Australia. Procedia Earth Planet. Sci. 7, 330–333.
Habermehl, M.A., 1980. The Great Artesian Basin, Australia. BMR (Bur. Miner. Resour.) J. Aust. Geol. Geophys. 5, 9–38.
Habermehl, M.A., 1986. Regional groundwater movement, hydrochemistry and hydrocarbon migration in the Eromanga Basin. Geological Society of Australia. In: In: Gravestock, D.I., Moore, P.S., Pitt, G.M. (Eds.), Contributions to the Geology and Hydrocarbon Potential of the Eromanga Basin, vol. 12. Geological Society of. Australia, pp. 353–376 Special Publication.
Habermehl, M.A., 2002. Hydrogeology, Hydrochemistry and Isotope Hydrology of the Great Artesian Basin. Bureau of Rural Sciences, Water Science Program, Canberra, ACT.
Hamilton, S.K., Esterle, J.S., Golding, S.D., 2012. Geological interpretation of gas content trends, Walloon Subgroup, eastern Surat Basin, Queensland, Australia. Int. J. Coal Geol. 101, 21–35.
Hamilton, S.K., Golding, S.D., Baublys, K., Esterle, J.S., 2014a. Stable isotopic and molecular composition of desorbed coal seam gases from the Walloon Subgroup, eastern Surat Basin, Australia. Int. J. Coal Geol. 122, 21–36.
Hamilton, S.K., Esterle, J.S., Sliwa, R., 2014b. Stratigraphic and depositional framework of the Walloon subgroup, eastern Surat Basin, Queensland. Aust. J. Earth Sci. 61, 1061–1080.
Hamilton, S.K., Golding, S.D., Baublys, K., Esterle, J.S., 2015. Conceptual exploration targeting for microbially enhanced coal bed methane (MECoM) in the Walloon Subgroup, eastern Surat Basin, Australia. Int. J. Coal Geol. 138, 68–82.
Hearn, S.J., Webb, J.P., 1984. Relative teleseismic P residuals and upper mantle structure in eastern Queensland, Australia. Bull. Seismol. Soc. Am. 74 (5), 1661–1681.
Hodgkinson, J., Grigorescu, M., 2013. Background research for selection of potential geostorage targets–case studies from the Surat Basin, Queensland. Aust. J. Earth Sci. 60, 71–89.
Hodgkinson, J., Hortle, A., McKillop, M., 2010. The application of hydrodynamic analysis in the assessment of regional aquifers for carbon geostorage: preliminary results for the Surat Basin, Queensland. APPEA J. 50th Anniv. Issue 445–462.
Jell, P.A., Draper, J.J., McKellar, J., 2013. Geology of Queensland: 7.1. Great Australian Superbasin. Geological Survey of Queensland, Brisbane.
Johannesson, K.H., Farnham, I., Guo, C., Stetzenback, K., 1999. Rare earth element fractionation and concentration variations along a groundwater flow path within a shallow, basin-fill aquifer, southern Nevada, USA. Geochim. Cosmochim. Acta 63 (18), 2697–2708.
Klohn Crippen Berger (KCB), 2017. Senex - western Surat gas project. Groundwater technical report, final. https://www.senexenergy.com.au/wp-content/uploads/2017/07/Appendix-F-KCB-WSGP-Groundwater-Report-1.pdf.
Kendall, C., McDonnell, J.J. (Eds.), 1998. Isotope Tracers in Catchment Hydrology (1998). Elsevier Science B.V., Amsterdam, pp. 839.
Korsch, R., Totterdell, J., Fomin, T., Nicoll, M., 2009. Contractional structures and deformational events in the bowen, Gunnedah and Surat basins, eastern Australia. Aust. J. Earth Sci. 56, 477–499.
Lagendijk, E., Ryan, D., 2010. From CSG to LNG: modeling and understanding key subsurface uncertainties for the development of a Surat Basin opportunity. In: Queensland, Australia. Paper Presented at SPE Canadian Unconventional Resources & International Petroleum Conference, Calgary, https://doi.org/10.2118/137651-MS. CSUG/SPE 137651.
Lemarchand, D., Jacobson, A.D., Cividini, D., Chabaux, F., 2015. The major ion, 87Sr/86Sr, and δ11B geochemistry of groundwater in the Wyodak-Anderson coal bed aquifer (Powder River Basin, Wyoming, USA). Compt. Rendus Geosci. 347 (7–8) 348.
Love, A.J., Karlstrom, K., Crossey, L., Rousseau-Gueutin, Priestley, S., Shand, P., Fluin, J., 2010. Geochemical and neo-tectonic data provide new understanding of the hydrogeology of the Great Artesian basin: ISARM2010. In: International Conference "Transboundary Aquifers: Challenges and New Directions", Proceedings.
Martin, M.A., Wakefield, M., MacPhail, M.K., Pearce, T., Edwards, H.E., 2013. Sedimentology and stratigraphy of an intra-cratonic basin coal seam gas play: Walloon Subgroup of the Surat Basin, eastern Australia. Petrol. Geosci. 19, 21–38.
Martinez, J.L., Raiber, M., Cox, M.E., 2015. Assessment of groundwater–surface water interaction using long-term hydrochemical data and isotope hydrology: headwaters of the Condamine River, Southeast Queensland, Australia. Sci. Total Environ. 536, 499–516.
McIntosh, J.C., Walter, L.M., Martini, A.M., 2002. Pleistocene recharge to midcontinent basins: effects on salinity structure and microbial gas generation. Geochem. Cosmochim. Acta 66, 1681–1700.
McIntosh, J.C., Walter, L.M., Martini, A.M., 2004. Extensive microbial modification of formation water geochemistry: case study from a Midcontinent sedimentary basin, United States. Geol. Soc. Am. Bull. 116, 743–759.
McKellar, J.L., 1998. Late Early to Late Jurassic Palynology, Biostratigraphy and Palaeogeography of the Roma Shelf Area, Northwestern Surat Basin, Queensland, Australia. PhD Thesis. The University of Queensland, Brisbane, Queensland, Australia 515 pp.
McKillop, M., Dixon, O., Hodgkinson, J., 2011. A new interpretation and model of the Moonie-Goondiwindi and Burunga-Leichhardt fault systems in Queensland. Geological Survey of Queensland Record 2011/1, Report 90318. https://www.business.qld.gov.au/industries/mining-energy-water/resources/minerals-coal/online-services/qdex-reports.
Moore, D.M., Reynolds Jr., R.C., 1997. X-Ray Diffraction and the Identification and Analysis of Clay Minerals, second ed. 400 pp.

Negrel, P., Petelet-Giraud, E., Millot, R., 2017. Sr isotopes as mixing and lithological tracers; the Ebro River Basin. Procedia Earth Planet. Sci. 17, 782–785.
Negrel, P., Casanova, J., Aranyossy, J.-F., 2001. Strontium isotope systematics used to decipher the origin of groundwaters sampled from granitoids: the Vienne Case (France). Chem. Geol. 177 (3–4), 287–308.
Office of Groundwater Impact Assessment (OGIA), 2016. Underground Water Impact Report for the Surat Cumulative Management Area. State of Queensland, Department of Natural Resources and Mines. https://www.dnrm.qld.gov.au/_data/assets/pdf_file/0007/345616/uwir-surat-basin-2016.pdf.
Owen, D.D.R., Cox, M.E., 2015. Hydrochemical evolution within a large alluvial groundwater resource overlying a shallow coal seam gas reservoir. Sci. Total Environ. 523, 233–252.
Worley Parsons, 2010. Australia pacific LNG project, Volume 5: Attachments. Attachment 21: ground water technical report – gas fields. http://www.aplng.com.au/pdf/eis/Volume_5/Vol5_Att_21-GroundWater_Gasfields.pdf, Accessed date: 16 February 2013.
Pashin, J.C., McIntyre-Redden, M.R., Mann, S.D., Kopaska-Merkel, D.C., Varonka, M., Orem, W., 2014. Relationships between water and gas chemistry in mature coalbed methane reservoirs of the Black Warrior Basin. Int. J. Coal Geol. 126, 92–105.
Petelet-Giraud, E., Negrel, P., Casanova, J., 2017. Tracing mixings and water-rock interactions in the loire River Basin (France): $\delta^{18}O$-$\delta^{2}H$ and $^{87}Sr/^{86}Sr$. Procedia Earth Planet. Sci. 17, 794–797.
Queensland Gas Company (QGC), 2013. 9.0 – a preliminary hydrochemistry model and isotope assessment. http://www.shell.com.au/about-us/projects-and-locations/qgc/environment/water-management/reports/_jcr_content/par/expandablelist_48b1/expandablesection_ea.stream/1498083768433/5f82e728b87ea57a23cb76b3e17e835681192679122551 3f82db52276b55fa32/qgc-stage-3-wmmp-dec-13-9.pdf.
Queensland Water Commission (QWC), 2012. Draft Underground Water Impact Report: Surat Cumulative Management Area. Consultation Draft. May 2012. Brisbane.
Radke, B.M., Ferguson, J., Cresswell, R.G., Ransley, T.R., Habermehl, M.A., 2000. Hydrochemistry and Implied Hydrodynamics of the Cadna-owie-hooray Aquifer Great Artesian Basin. B. O. R. Sciences. Australia. Bureau of Rural Sciences, Canberra 248.
Ransley, T., Somerville, P., Tan, K.P., Feitz, A., Cook, S., Yates, G., Schoning, G., Bell, J., Caruana, L., Sundaram, S., Wallace, L., 2015. Groundwater Hydrochemical Characterisation of the Surat Region and Laura Basin - Queensland. Geoscience Australia, Canberra Record 2015/05. https://doi.org/10.11636/Record.2015.005.
Rice, C.A., Flores, R.M., Stricker, G.D., Ellis, M.S., 2008. Chemical and stable isotopic evidence for water/rock interaction and biogenic origin of coalbed methane, Fort Union Formation, Powder River Basin, Wyoming and Montana U.S.A. Int. J. Coal Geol. 76, 76–85.
Ryan, D.J., Hall, A., Erriah, L., Wilson, P.B., 2012. The Walloon coal seam gas play, Surat Basin, Queensland. APPEA J. 52, 273–289.
Saygin, E., Kennett, B.L., 2010. Ambient seismic noise tomography of Australian continent. Tectonophysics 481, 116–125.
Scott, S., Anderson, B., Crosdale, P., Dingwall, J., Leblang, G., 2004. Revised geology and coal seam gas characteristics of the Walloon Subgroup – Surat Basin, Queensland. In: Boult, P.J., Johns, D.R., Lang, S.C. (Eds.), Eastern Australasian Basins Symposium II. Petroleum Exploration Society of Australia, Special Publication, pp. 345–355.
Scott, S., Anderson, B., Crosdale, P., Dingwall, J., Leblang, G., 2007. Coal petrology and coal seam gas contents of the Walloon Subgroup – Surat Basin, Queensland, Australia. Int. J. Coal Geol. 70, 209–222.
Sliwa, R., Esterle, J., 2008. Re-evaluation of structure and sedimentary packages in the eastern Surat Basin. In: Blevin, J.E., Bradshaw, B.E., Uruski, C. (Eds.), Eastern Australasian Basins Symposium III. Petroleum Exploration Society of Australia, pp. 527 Special Publication.
Stueber, A.M., Walter, L.M., Huston, T.J., Pushkar, P., 1993. Formation waters from Mississippian-Pennsylvanian reservoirs, Illinois basin, USA - Chemical and isotopic constraints on evolution and migration. Geochimica Et Cosmochimica Acta 57 (4), 763–784.
Stueber, A.M., Walter, L.M., 1991. Origin and chemical evolution of formation waters from silurian-devonian strata in the Illinois Basin, USA. Geochim. Cosmochim. Acta 55 (1), 309–325.
Stueber, A.M., Pushkar, P., Hetherington, E.A., 1987. A strontium isotopic study of formation waters from the Illinois basin, USA. Appl. Geochem. 2 (5–6), 477–494.
Suckow, A., Raiber, M., Deslandes, A., Gerber, C., 2018. Constraining Conceptual Groundwater Models for the Hutton and Precipice Aquifers in the Surat Basin through Tracer Data. CSIRO, Australia Final Report.
Veizer, J., 1989. Strontium isotopes in seawater through time. Annu. Rev. Earth Planet Sci. 17 (1), 141–167.
Van Voast, W.A., 2003. Geochemical signature of formation waters associated with coalbed methane. AAPG (Am. Assoc. Pet. Geol.) Bull. 87, 667–676.
Wahlberg, J.S., Baker, J.H., Vernon, R.W., Dewar, R., 1965. Exchange Adsorption of Strontium on Clay Minerals. US Govt. Print. Off.
Willink, R., 2008. Comparative Geological Setting of Conventional Oil and Gas Fields and CSG Resources in the Surat/Bowen Basin, Queensland. Eastern Australasian Basins Symposium III. Petroleum Exploration Society of Australia on cd.